CONTROL OF ELECTROMAGNETIC SCATTERING BY ANTENNA IMPEDANCE LOADING

Shi-Chuan Lee

Ohio State University

Prepared for:

Air Force Cambridge Research Laboratories

July 1974

AFCRL-TR-74-0426

CONTROL OF ELECTROMAGNETIC SCATTERING BY ANTENNA IMPEDANCE LOADING

Shi-chuan Lee

The Ohio State University
ElectroScience Laboratory
Department of Electrical Engineering
Columbus, Ohio 43212

July 1974

Scientific Report No. 2

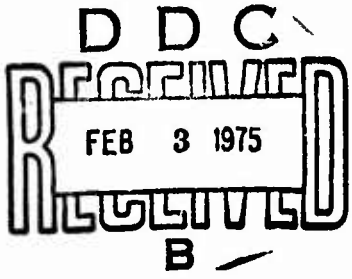

AIR FORCE CAMBRIDGE RESEARCH LABORATORIES
AIR FORCE SYSTEMS COMMAND
UNITED STATES AIR FORCE
HANSCOM AFB, MASSACHUSETTS 01731

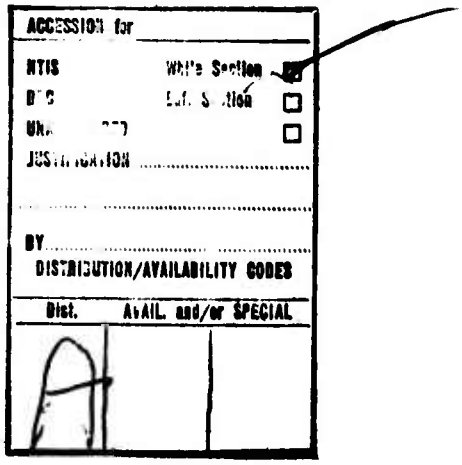

Qualified requestors may obtain additional copies from the Defense Documentation Center. All others should apply to the National Technical Information Service.

UNCLASSIFIED

SECURITY CLASSIFICATION OF THIS PAGE (When Data Entered)

REPORT DOCUMENTATION PAGE

READ INSTRUCTIONS BEFORE COMPLETING FORM

1. REPORT NUMBER: AFCRL-TR-74-0426	2. GOVT ACCESSION NO.
3. RECIPIENT'S CATALOG NUMBER: AD/A-004134	
4. TITLE (and Subtitle): CONTROL OF ELECTROMAGNETIC SCATTERING BY ANTENNA IMPEDANCE LOADING	5. TYPE OF REPORT & PERIOD COVERED: Scientific Report No. 2
	6. PERFORMING ORG. REPORT NUMBER: ESL 3424-2
7. AUTHOR(s): Shi-chuan Lee	8. CONTRACT OR GRANT NUMBER(s): F19628-72-C-0203
9. PERFORMING ORGANIZATION NAME AND ADDRESS: The Ohio State University ElectroScience Laboratory, Department of Electrical Engineering, Columbus, Ohio 43212	10. PROGRAM ELEMENT, PROJECT, TASK AREA & WORK UNIT NUMBERS: 5635-02-01, 61102F, 681305
11. CONTROLLING OFFICE NAME AND ADDRESS: Air Force Cambridge Research Laboratories, Hanscom AFB, Massachusetts 01731, Contract Monitor: John K. Schindler/LZR	12. REPORT DATE: July 1974
	13. NUMBER OF PAGES: 81
14. MONITORING AGENCY NAME & ADDRESS (if different from Controlling Office)	15. SECURITY CLASS. (of this report): Unclassified
	15a. DECLASSIFICATION/DOWNGRADING SCHEDULE

16. DISTRIBUTION STATEMENT (of this Report)

Approved for public release; distribution unlimited.

17. DISTRIBUTION STATEMENT (of the abstract entered in Block 20, if different from Report)

18. SUPPLEMENTARY NOTES

TECH, OTHER

19. KEY WORDS (Continue on reverse side if necessary and identify by block number)

Radar scattering
Cross section reduction
Impedance loading
Numerical analysis
Edge diffraction

20. ABSTRACT (Continue on reverse side if necessary and identify by block number)

The application of impedance loading techniques for the reduction of backscatter from radar targets were studied. The hybrid methods which combine the GTD and the moment method were used to analyze the backscattering from various geometries such as impedance loaded infinite wedge and a two-dimensional wing model. The effect of both the trailing and the leading edge was considered by using a two-

DD FORM 1 JAN 73 1473 EDI

UNCLASSIFIED

SECURITY CLASSIFICATION OF THIS PAGE (When Data Entered)

ACKNOWLEDGMENTS

The author wishes to express sincere appreciation to his adviser, Professor Roger C. Rudduck, for his constant guidance, suggestions and encouragement on this dissertation, including the idea for the modified hybrid (ΔJ) method. Appreciation is also expressed to Professor Leon Peters, Jr. for his reading of the manuscript and constructive suggestions. Special thanks are extended to Professor Jack H. Richmond for critically reviewing the manuscript and making his computer programs available to the author. The author would also like to extend his thanks to all his colleagues at the ElectroScience Laboratory and in particular to Dr. W. D. Burnside for his helpful suggestions. The support of the Air Force Cambridge Research Laboratory under Contract F19628-72-C-0203 is greatly appreciated.

The material contained in this report is also used as a dissertation submitted to the Department of Electrical Engineering, The Ohio State University as partial fulfillment for the degree Doctor of Philosophy.

20.

dimensional wing model. The edge diffraction source can be considerably reduced over a 3:1 frequency band for the two-dimensional case. The square plate with a loaded slot was analyzed by a wire grid model. The backscatter reduction of the square plate can be achieved at least over a 2:1 frequency band.

TABLE OF CONTENTS

CHAPTER I
INTRODUCTION

This chapter contains a statement of the problem considered in the dissertation, the motivation for considering the problem, a summary of the contents, and a brief survey of the literature on the control of electromagnetic scattering from radar targets.

The objective of the research reported herein is to investigate the application of impedance loading techniques for the reduction of backscatter from radar targets. A primary goal is to achieve techniques for minimizing backscatter by controlling edge diffraction sources. Edges are major contributors to backscattering for many scattering geometries such as wing structures and finite conical shapes.

The suppression of scattering is a camouflage problem, but over the years the development of techniques for the reduction of specular contributions has received most attention. Although the specular contributions tend to be restricted in the aspect angles for which they occur, they dominate the net return whenever they are present. However, the specular echoes are amenable to suppression using radar absorbers. On the other hand, non-specular scattering is more pervasive. Even if all specular echoes are suppressed, the non-specular scattering still can generate radar returns of unacceptable magnitude. In fact, modern aerospace vehicles are often not seen at specular aspects in a tactical environment. But the non-specular radar cross section can still reach levels that increase the probability of detection. It is therefore important to study the backscatter reduction for non-specular aspects.

In Chapter II the impedance boundary condition and the integral equations appropriate in an antenna and scattering problem are examined. The low frequency numerical technique, the method of moments, and the high frequency wedge diffraction theory are also discussed. These theories provide the necessary theoretical background for the applications in the later chapters.

Chapter III presents the hybrid methods which combine the Geometrical Theory of Diffraction (GTD) and the Method of Moments. These hybrid methods can be used to treat problems which can not be solved by either GTD or moment method alone.

In Chapter IV, the hybrid methods are applied to study the back-scatter reduction from various geometries such as the infinite wedge, the thin strip and a two-dimensional wing model. The loadings required for optimum reduction are also shown.

In Chapter V, the scattering from a thin square plate loaded with a slot has been studied as a way of implementing the required antenna impedance loading. The effect of loading as a function of frequency is also presented.

A considerable amount of effort has been devoted to the reduction of backscatter from various radar target geometries [1,2,3,4] over the years. For modifying the radar cross section of scattering bodies, two techniques have been used either separately or jointly; shaping of the body and coating of the body with radar absorber. Recently, the surface impedance model of absorber and the integral equations were used by Knott et al. [5,6,7] to study the nor-specular radar cross section.

A more encouraging method of reducing radar cross section is the antenna impedance loading techniques [8,9]. The scattering from a conducting object can be controlled by loading portions of its surface with distributed or lumped impedances. The scattered field from a loaded object can be expressed as a superposition of fields scattered by the unloaded object and fields reradiated by the loading. The interference of these fields can therefore be used to control the scattering. The impedance loading technique has been applied to dipole, cylindrical and loop antennas to minimize the radar cross section [10,31]. The backscatter reduction in the broadside direction for a small plate loaded with an open or short circuited slot was investigated by Green [32].

CHAPTER II
THEORETICAL BACKGROUND

A. Introduction

In this chapter the impedance boundary condition and the integral equations appropriate in an antenna and scattering problem will be examined. The purpose of this study is to show how the equations are affected by the geometry and the boundary conditions. A general procedure for solving linear equations, the method of moments, will be discussed. The wedge diffraction solution, which is a very important part of the Geometrical Theory of Diffraction, is also presented. Each of these solutions are presented in their basic terms in this chapter and applied to specific problems in the following chapters.

B. The Impedance Boundary Conditions

In its most straightforward form an impedance boundary condition [11] is one which relates the tangential components of the electric and magnetic fields via an impedance factor. The impedance factor itself is a function of the properties of the surface. The conditions are widely used in diffraction problems and the analysis of surface wave phenomena. In this dissertation, the surface impedance is employed to represent a loaded slot. Consider a closed cylindrical surface whose generators are parallel to the z axis of a cylindrical coordinate system and whose profile in a plane perpendicular to the z axis is the closed curve c. Let $\hat{n}$ be an outward unit vector to c and let $\hat{t}$ be a unit vector in the tangential direction, such that $\hat{t}$, $\hat{n}$ and $\hat{z}$ form a right-hand system. Then, on the surface, the impedance boundary condition is given by [12,13]

$$\vec{E} - (\hat{n}\cdot\vec{E})\hat{n} = Z_s\, \hat{n} \times \vec{H} \tag{1}$$

where $\vec{E}$ and $\vec{H}$ are the total electric and magnetic field, respectively, in the region surrounding the body, which is that of free space for the radar environment and Z_s is the surface impedance. Z_s may be a function of distance t along the cylindrical surface c. For a perfectly conducting surface, $Z_s = 0$. Equation (1) can alternatively be expressed as [12,13]

$$\vec{H} - (\hat{n}\cdot\vec{H})\hat{n} = -\frac{1}{Z_s}\, \hat{n} \times \vec{E} \tag{2}$$

Equation (2) is the dual of Eq. (1) and is not valid if at any point on the surface Z_s is zero.

C. The Reaction Integral Equation

The reaction concept and its applications have been discussed by Rumsey [14], Cohen [15], Harrington [16] and Richmond [17]. The reaction integral equation has been used extensively by Richmond [19, 30,33].

Let us consider the application of Schelkunoff's surface equivalence principle [18] to the exterior scattering problem illustrated in Fig. 1a. In the presence of a dielectric or conducting body, the external electric and magnetic currents $(\vec{J}_i, \vec{M}_i)$ generate the electric and magnetic field intensities $(\vec{E}, \vec{H})$. For convenience, assume the exterior medium is free space.

According to the equivalence principle, if we introduce the following surface current densities

$$\vec{J}_s = \hat{n} \times \vec{H} \tag{3}$$

$$\vec{M}_s = \vec{E} \times \hat{n} \tag{4}$$

on the closed surface S of the scatterer, the interior field will vanish, without disturbing the exterior field. Since the field internal to S is zero, as illustrated in Fig. 1b, we can replace the scatterer by free space without disturbing the field anywhere. By definition, the incident field $(\vec{E}_i, \vec{H}_i)$ is generated by the external source $(\vec{J}_i, \vec{M}_i)$ in free space, and the scattered field is:

$$\vec{E}_s = \vec{E} - \vec{E}_i \tag{5}$$

$$\vec{H}_s = \vec{H} - \vec{H}_i \ . \tag{6}$$

From the superposition principle and the uniqueness theorem, we know that the surface current $(\vec{J}_s, \vec{M}_s)$ which radiates in free space will generate the field $(\vec{E}_s, \vec{H}_s)$ in the exterior and $(-\vec{E}_i, -\vec{H}_i)$ in the interior region, as shown in Fig. 1c.

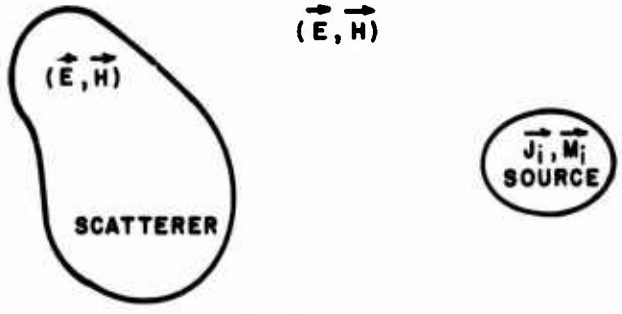

Fig. 1a--The source $(\vec{J}_i,\vec{M}_i)$ generates the field $(\vec{E},\vec{H})$ with scatterer.

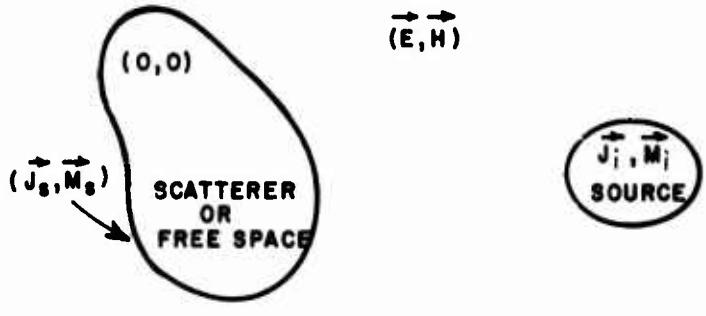

Fig. 1b--The interior field vanishes when the current $(\vec{J}_S,\vec{M}_S)$ are introduced on the surface of the scatterer.

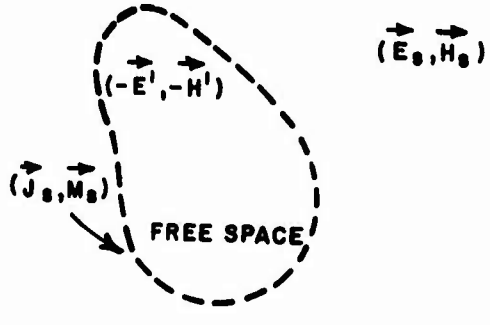

Fig. 1c--The exterior scattered field may be generated by $(\vec{J}_S,\vec{M}_S)$ in free space.

With the scatterer replaced by free space and the equivalent current on its surface S, we have noted in Fig. 1b that the interior region has a zero field. Now let us place a test source or probe in the interior region, as shown in Fig. 2, and consider its reaction with the other sources. If the test source has electric current density $\vec{J}_t$ and magnetic current density $\vec{M}_t$, the reaction principle gives

$$(7) \qquad \iint (\vec{J}_t \cdot \vec{E}_s - \vec{M}_t \cdot \vec{H}_s) ds = - \iint (\vec{J}_t \cdot \vec{E}_i - \vec{M}_t \cdot \vec{H}_i) ds$$

where $(\vec{E}_s, \vec{H}_s)$ is the scattered field generated by $(\vec{J}_s, \vec{M}_s)$, and the integrals extend over the surface of the test source. Equation (7) is one form of the reaction integral equation (RIE). As noted by Richmond [19], the RIE is more general than the electric field integral equation (EFIE) or the magnetic field integral equation (MFIE). If we enforce Eq. (7) with a set of delta-function electric test sources, the RIE reduces to the EFIE. If we enforce Eq. (7) with a set of delta-function magnetic test sources, the RIE reduces to the MFIE.

From Eq. (7) and the reciprocity theorem, we obtain another form of the reaction integral equation:

$$(8) \qquad \oiint_S (\vec{J}_s \cdot \vec{E}_t - \vec{M}_s \cdot \vec{H}_t) ds + \iiint (\vec{J}_i \cdot \vec{E}_t - \vec{M}_i \cdot \vec{H}_t) dv = 0$$

where $(\vec{E}_t, \vec{H}_t)$ is the field of the test source radiating in free-space. In words, Eq. (8) states that the interior test source has zero reaction with the other sources. This zero-reaction was developed by Rumsey [14].

Combining the impedance boundary condition, Eq. (1), with the equivalent current equations, Eqs. (3) and (4), gives:

$$(9) \qquad \vec{M}_s = Z_s \vec{J}_s \times \hat{n} .$$

Equation (9) is another form of the impedance boundary condition. For two-dimensional problems involving cylindrical scatterers, $\vec{J}_s$ and $\vec{M}_s$ are functions only of the position t around the cylindrical surface c. If $\vec{J}_i$ vanishes, Eqs. (8) and (9) yield

$$(10) \qquad \oint_c \vec{J}_s \cdot [\vec{E}_t - (\hat{n} \times \vec{H}_t) Z_s] dt = \iint \vec{M}_i \cdot \vec{H}_t \, ds.$$

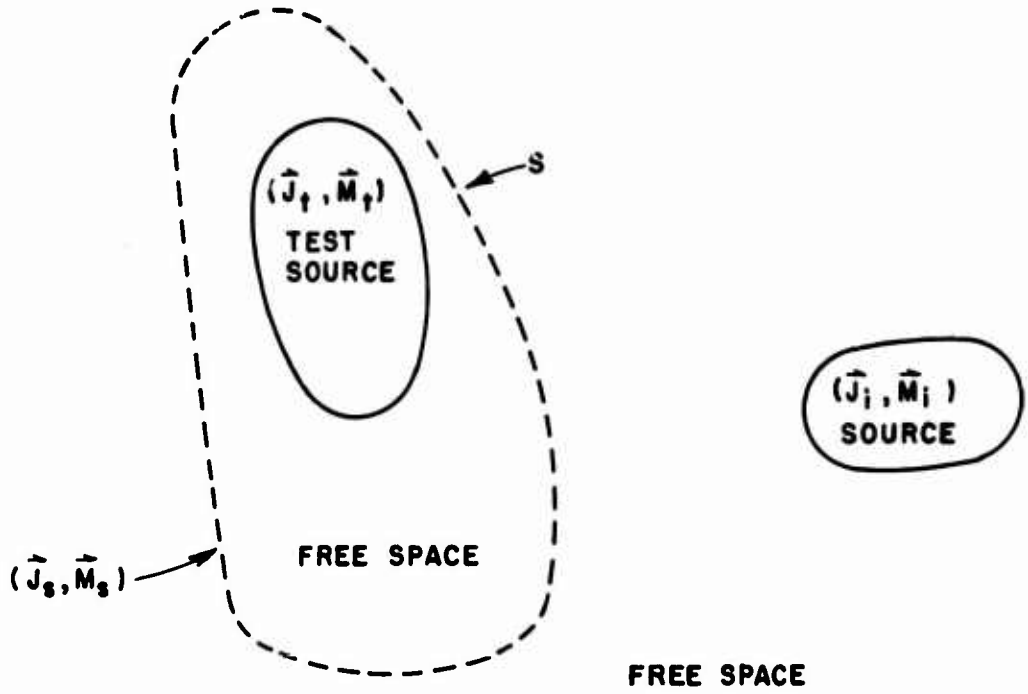

Fig. 2--A test source $(\vec{J}_t, \vec{M}_t)$ is placed in the interior region of the scatterer.

D. Method of Moments

The method of moments [20] is a general procedure for solving integral equations. It is widely used, with the help of high speed digital computers, in solving low-frequency electromagnetic antenna and scattering problems. Consider the linear inhomogeneous equation

$$L_{op}\,(\vec{J}) = \vec{E} \tag{11}$$

where L_{op} is a linear operator, $\vec{E}$ is a known excitation function or source, and $\vec{J}$ is the unknown response function to be determined. Equation (11) may be the RIE, EFIE or MFIE.

The procedure for obtaining an approximate solution to Eq. (11) can be summarized as below. First, expand the unknown function in a series of basis functions in the domain of the operator L_{op}, as

$$\vec{J} = \sum_{n}^{N} \alpha_n \vec{J}_n \,. \tag{12}$$

Substituting Eq. (12) into (11) gives

$$(13) \qquad \sum_{n}^{N} \alpha_n L_{op} (\vec{J}_n) = \vec{E} .$$

The next step is to define a set of weighting functions $\vec{w}_1, \vec{w}_2 \cdots$ in the domain of L_{op} and then form the inner product

$$(14) \qquad \sum_{n} \alpha_n < \vec{w}_m, L_{op} \vec{J}_n > = < \vec{w}_m, \vec{E} >.$$

Equation (14) is a set of linear equations which can be solved for the unknown α_n by numerical techniques.

Two special cases of the moment method are of particular importance in electromagnetics, namely; the Galerkin's method and the point matching technique. The Galerkin's method uses the same set of functions as the expansion and weighting functions. It requires the evaluation of integrals which may be tedious and computationally expensive. This difficulty can be minimized if one uses point matching which uses the Dirac delta functions as testing functions.

E. Wedge Diffraction

Wedge diffraction is a useful tool in the analyses of high-frequency electromagnetic problems. The asymptotic solution for the diffraction from a conduting wedge was first obtained by Sommerfeld [21]. Originally, GTD [34] as applied to diffraction by a wedge was based on plane wave diffraction coefficients; however, as shown by Russo, Rudduck and Peters in Refs. [22,41], the use of diffraction of cylindrical waves has been found necessary in the treatment of antennas. Consequently, different formulations of wedge diffraction were substituted for the plane wave diffraction coefficient which is the basis for wedge diffraction theory. Pauli [23] introduced the V_B function as a practical formulation to the solution for a finite-angle conducting wedge. Recently, however, Hutchins and Kouyoumjian[24, 25] presented a formulation for the diffracted field (V_B), which significantly improves the accuracy over that obtained from Pauli's form.

This improved diffraction solution [24,25] is better in the transition regions (near the incident and refleted shadow boundaries). It can be written in the form

$$(15) \qquad V_B(L,\beta,n) = I_{-\pi}(L,\beta,n) + I_{+\pi}(L,\beta,n)$$

where

$$I_{\pm\pi}(L,\beta,n) \sim \frac{e^{-j(kL+\pi/4)}}{jn\sqrt{2\pi}} \sqrt{a}\, \cot\, \frac{\pi\pm\beta}{2n} \quad x$$

$$e^{jkLa} \int_{(kLa)^{1/2}}^{\infty} e^{-j\tau^2}\, d\tau + [\text{higher order terms}]$$

where the higher order terms are negligible for large kr and with n defined from the wedge angle WA $=(2-n)\pi$, also $a = 1 + \cos(\beta - 2n\pi N)$ and N is a positive or negative integer or zero, whichever most nearly satisfies the equations

$$2n\pi N - \beta = -\pi \quad \text{for } I_{-\pi}$$

$$2n\pi N - \beta = +\pi \quad \text{for } I_{+\pi} \ .$$

Consider a plane electromagnetic wave normally incident on a wedge of angle $(2-n)\pi$ as illustrated in Fig. 3. Cylindrical coordinates are employed here with the z-axis coincident with the edge and consequently normal to the plane of diffraction. The z-component of the total field at observation point $P(r,\psi)$ may be represented by the scalar function u, given by

$$(16) \qquad u(r,\psi,n) = V(r,\psi-\psi_0,n) \pm V(r,\psi+\psi_0,n) \ .$$

The minus sign applies for the boundary condition u = 0 on the wedge surface; thus the solution is valid for the electric field oriented in the z-direction (parallel to the edge). The plus sign applies for the normal derivative of u equal zero on the wedge surface, or the magnetic field oriented in the z-direction (polarization perpendicular to the edge). The quantities $V(r,\phi,n)$ represent the separation of the solution into incident and reflected waves and are given by

$$(17) \qquad V(r,\phi,n) = V^*(r,\phi,n) + V_B(r,\phi,n)$$

where V* is the geometrical optics wave which is given by

$$(18) \qquad V^*(r,\phi,n) = \begin{cases} \exp[jkr\cos(\phi+2\pi nN)], & \text{if } -\pi<\phi+2\pi nN<\pi \\ & \text{for } N=0, \pm1, \pm2 \cdots \\ 0, & \text{otherwise.} \end{cases}$$

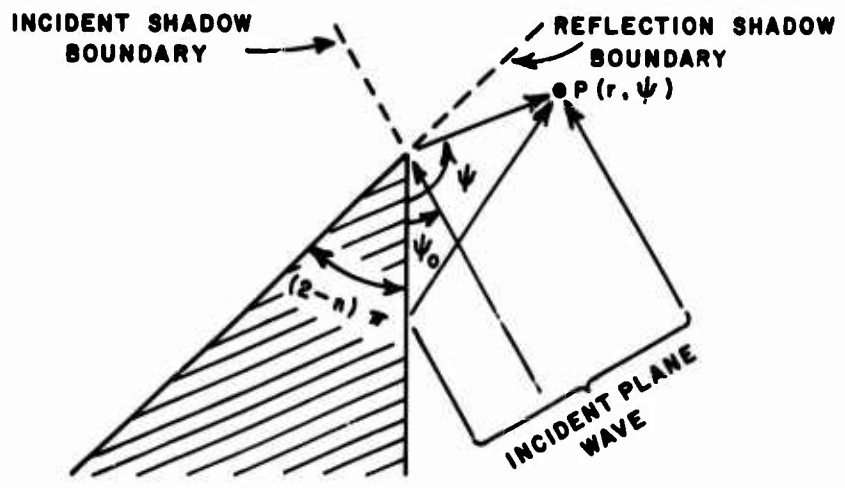

Fig. 3--Diffraction of a plane wave by a conducting wedge.

CHAPTER III
HYBRID METHODS

A. Introduction

For many years, GTD has been applied to high-frequency antenna and scattering problems for which the structure is large in terms of wavelength. GTD solutions have mainly been used in pattern computations with little information concerning antenna impedance and/or aperture distribution. This is especially true for wire-type antennas. On the other hand, the method of moment has been applied to low-frequency problems for which the structure is small in terms of wavelength.

A hybrid method (MMGTD) to combine the GTD and the Moment Method was used by Burnside [27,28] to investigate the scattering of a TE plane wave by infinite conducting structures. In this chapter, the original hybrid method is extended to treat infinite geometries with local inhomogenities which can not be solved by either GTD or moment method alone. While the method gives good results for finite geometries, it fails to predict the fields of infinite structures accurately. A modified hybrid method, which is more accurate and economical in computation, is introduced. The modified method can be applied to geometries with local surface impedance if the surface current density for the conducting case is known. The modified method was first suggested by Rudduck.

B. A Hybrid Method

Consider the scattering by a simple perfectly conducting wedge for a TE plane wave incident as shown in Fig. 4. At the field point (ρ,ψ), the incident field is given by

$$H_z^i(\rho,\psi) = e^{jk\rho\cos(\psi-\psi_0)} \qquad \text{for } |\psi-\psi_0| < 180^\circ .$$

The reflected field from the wall along the x-axis of Fig. 4 is given by

$$H_z^r(\rho,\psi) = e^{jk\rho\cos(\psi+\psi_0)} \qquad \text{for } |\psi+\psi_0| < 180^\circ$$

The diffracted field can be expressed as [26]

$$H_z^d(\rho,\psi) = V_B(\rho,\psi-\psi_0,n) + V_B(\rho,\psi+\psi_0,n).$$

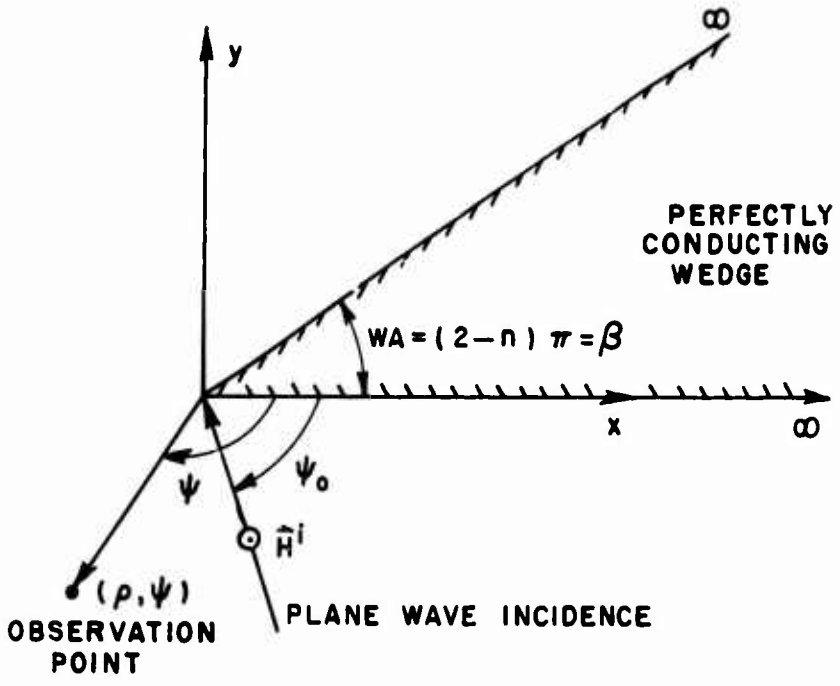

Fig. 4--Plane wave diffraction by conducting wedge.

If the observation point is not in the vicinity of a shadow boundary ($\psi \pm \psi_0 = 180°$) and for ρ sufficiently large, the diffracted field can be expressed by [26]

$$H_z^d(\rho,\psi) \approx [D(\psi-\psi_0,n) + D(\psi+\psi_0,n)] \frac{e^{-jk\rho}}{\sqrt{\rho}} \tag{19}$$

where

$$D(\phi,n) = \frac{e^{-j\frac{\pi}{4}}}{\sqrt{2\pi k}} \left[\frac{\frac{1}{n} \sin \frac{\pi}{n}}{\cos \frac{\pi}{n} - \cos \frac{\phi}{n}} \right]$$

is the asymptotic diffraction coefficient in GTD. The total magnetic field can then be expressed, using the above form of the diffracted field, by

$$(20) \qquad H_z^t(\rho,\psi) = H_z^i + H_z^r + H_z^d$$

$$\approx H_z^i + H_z^r + C(\psi,\psi_0,n)\,\frac{e^{-jk\rho}}{\sqrt{\rho}}$$

where C is independent of the range (ρ). The total surface current density on a perfectly conducting surface can be obtained by applying the boundary conditions, and is given by

$$\vec{J} = (\hat{n} \times \hat{z})H_z^t$$

where $\hat{n}$ is the unit outward normal vector to the surface. Using the GTD solution for the total magnetic field, the total surface current density along the wedge walls is given, for ρ sufficiently large, by

$$(21) \qquad \vec{J}^{GTD} = (\hat{n} \times \hat{z})\,[H_z^i + H_z^r + H_z^d]$$

$$\simeq \vec{J}^i + \vec{J}^r + (\hat{n} \times \hat{z})\,C(\psi,\psi_0,n)\,\frac{e^{-jk\rho}}{\sqrt{\rho}}\,.$$

Equation (21) is also valid for wedges with local inhomogenities around the tip, assuming that the wedge surface is not in the vicinity of a shadow boundary and ρ is sufficiently far away from the local inhomogenities.

Note that C is now assumed to be an unknown constant, although it can be obtained from a canonical solution for the perfectly conducting case. The hybrid approach can be applied to a set of problems where the coefficient C is not known at the outset.

The magnetic field integral equation for cylinders with arbitrary anisotropic surface impedance is given by [29]

$$(22) \qquad -H_z^i(s') = \frac{1}{2}\,J(s') + \frac{k}{4}\int_S \frac{Z_s}{\eta_0} J_s(s)\; H_0^{(2)}(k|\vec{\rho}\,' - \vec{\rho}\,|)\,ds$$

$$+ \frac{jk}{4}\int_S J_s(s)\;\frac{(\vec{\rho}\,' - \vec{\rho})\cdot\hat{n}}{|\vec{\rho}\,' - \vec{\rho}\,|}\; H_1^{(2)}(k|\vec{\rho}\,' - \vec{\rho}\,|)\,ds$$

where the time dependence is assumed to be $e^{+j\omega t}$ and is suppressed, the integrals are extended over the contour S of the cylinder cross section,

$\hat{n}$ is the outward normal to the contour S, and η_0 is the intrinsic impedance of free space. Consider the impedance-loaded wedge structure as illustrated in Fig. 5, the total surface current density can be defined by

$$(23)\qquad J = \begin{cases} J_h^{GTD} & h_c \le h \le \infty \quad \text{on h-wall} \\ J_h^{MM} & 0 \le h \le h_c \quad \text{on h-wall} \\ J_x^{GTD} & x_c \le x \le \infty \quad \text{on x-wall} \\ J_x^{MM} & 0 \le x \le x_c \quad \text{on x-wall} \end{cases}$$

where J^{GTD} is defined by Eq. (21) which is valid only away from the impedance or the tip. The method of moment current (J^{MM}) around the inhomogenities can be defined by simple basis functions such as

$$(24)\qquad J^{MM} = \sum_{m=1}^{N} \alpha_m P_m(s-s_m)$$

where $P_m(s-s_m)$ are orthogonal pulse functions with weight α_m.

Applying the point matching technique at the midpoint of each of the N pulse segment, one obtains

$$(25)\qquad \sum_{m=1}^{N} \alpha_m \ell_{nm} + L_n(J_h^{GTD}) + L_n(J_x^{GTD}) = g_n \qquad \text{for } 1 \le n \le N$$

where

$$\ell_{nm} = \begin{cases} \dfrac{k}{4}\displaystyle\int_{ds_m}\left[\frac{Z_s}{\eta_0} H_0^{(2)}(k|\vec{\rho}_n-\vec{\rho}'|) + j\,\frac{(\vec{\rho}_n-\vec{\rho}')\cdot\hat{n}}{|\vec{\rho}_n-\vec{\rho}'|} H_1^{(2)}(k|\vec{\rho}_n-\vec{\rho}'|)\right]ds & m\neq n \\ \dfrac{1}{2} + \dfrac{k}{4}\,\dfrac{Z_s}{\eta_0}\,\Delta s_n\left[1 - j\,\dfrac{2}{\pi}\ln\left(\dfrac{\gamma k \Delta s_n}{4e}\right)\right] & m=n, \end{cases}$$

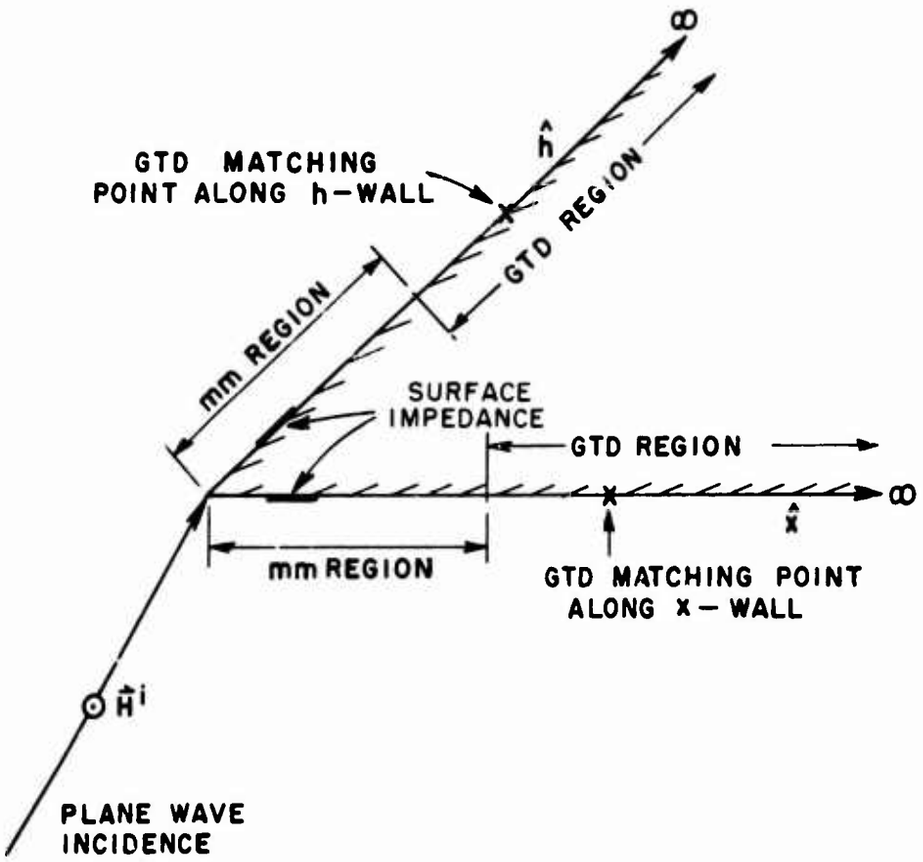

Fig. 5--Impedance loaded wedge applied in hybrid methods.

$e = 2.71828,$

$\gamma = 1.781..$ is the Euler's constant,

$g_n = -H_z^i (x_n, y_n)$

and

$$(26)\qquad L_n(J^{GTD}) = \frac{k}{4}\int_{S_{GTD}} J^{GTD}\left[\frac{Z_s}{\eta_o}\, H_o^{(2)}(k|\vec{\rho}_n-\vec{\rho}'|) + j\cdot\frac{(\vec{\rho}_n-\vec{\rho}')\cdot\hat{n}}{|\vec{\rho}_n-\vec{\rho}'|}\, H_1^{(2)}(k|\vec{\rho}_n-\vec{\rho}'|)\right] ds$$

Note that the first term in Eq. (26) vanishes because $Z_s = 0$ in the GTD region. Substituting Eq. (21) into Eq. (25) gives

$$(27)\qquad \sum_{m=1}^{N}\alpha_m \ell_{nm} + L_n\left(J_h^i + J_h^r + D_h\frac{e^{-jkh}}{\sqrt{h}}\right) + L_n\left(J_x^i + J_x^r + D_x\frac{e^{-jkx}}{\sqrt{x}}\right) = g_n \quad 1 \le n \le N$$

where the second term exists on the h-wall and the third term on the x-wall. Since the incident and reflected currents (J^i and J^r) can be easily obtained by geometrical optics, they can be transferred to the source side. Since D_x and D_h are just complex constants, by applying the linear property of the operator L_n, Eq. (27) can be written as

$$(28)\qquad \sum_{m=1}^{N}\alpha_m \ell_{mn} + D_h L_n\left(\frac{e^{-jkh}}{\sqrt{h}}\right) + D_x L_n\left(\frac{e^{-jkx}}{\sqrt{x}}\right) = g_n' \quad \text{for } 1 \le n \le N$$

where

$$g_n' = -H_z^i(x_n,y_n) - L_n(J_x^i+J_x^r) - L_n(J_h^i+J_h^r)$$

$$(29)\quad L_n\left(\frac{e^{-jkx}}{\sqrt{x}}\right) = \frac{k}{4}\int_{x_c}^{\infty}\left[\frac{Z_s}{\eta_o}\, H_o^{(2)}(k|\vec{\rho}_n-\vec{\rho}|) + j\,\frac{(\vec{\rho}_n-\vec{\rho})\cdot\hat{n}}{|\vec{\rho}_n-\vec{\rho}|}\, H_1^{(2)}(k|\vec{\rho}_n-\vec{\rho}|)\right] \times \frac{e^{-jkx'}}{\sqrt{x'}}\, dx'$$

$$(30)\quad L_n\left(\frac{e^{-jkh}}{\sqrt{h}}\right)=\frac{k}{4}\int_{\infty}^{h_c}\frac{Z_s}{\eta_o}H_o^{(2)}(k|\vec{\rho}_n-\vec{\rho}|)+j\,\frac{(\vec{\rho}_n-\vec{\rho})\cdot\hat{n}}{|\vec{\rho}_n-\vec{\rho}|}H_1^{(2)}(k|\vec{\rho}_n-\vec{\rho}|)$$

$$\times\frac{e^{-jkh'}}{\sqrt{h'}}\,dh'$$

$$(31)\quad L_n(J_x^i+J_x^r)=\begin{cases}2\displaystyle\int_{x_c}^{\infty}\frac{k}{4}\left[\frac{Z_s}{\eta_o}H_o^{(2)}(k|\vec{\rho}_n-\vec{\rho}|)+j\,\frac{(\vec{\rho}_n-\vec{\rho})\cdot\hat{n}}{|\vec{\rho}_n-\vec{\rho}|}H_1^{(2)}(k|\vec{\rho}_n-\vec{\rho}|)\right]\\ \qquad\times e^{jkx'\cos\psi_o}\,dx' \quad \text{for } 0^\circ\le\psi_o\le 180^\circ\\ 0 \qquad\qquad \text{otherwise}\end{cases}$$

$$(32)\quad L_n(J_{\parallel}^i+J_h^r)=\begin{cases}2\displaystyle\int_{\infty}^{h_c}\frac{k}{4}\left[\frac{Z_s}{\eta_o}H_o^{(2)}(k|\vec{\rho}_n-\vec{\rho}|)+j\,\frac{(\vec{\rho}_n-\vec{\rho})\cdot\hat{n}}{|\vec{\rho}_n-\vec{\rho}|}H_1^{(2)}(k|\vec{\rho}_n-\vec{\rho}|)\right]\\ \qquad\times e^{jkh'\cos(\beta-180^\circ+\psi_o)}\,dh' \quad \text{for } 180^\circ-\beta\le\psi_o\le 360^\circ-\beta\\ 0 \qquad\qquad \text{otherwise .}\end{cases}$$

So far, we only have N equations obtained by point matching in the moment method region. However, there are N+2 unknowns, N coefficients of the current pulses (α_n's) in the moment method region and two diffraction coefficients (D_x and D_h), one in each GTD region.

Two additional equations are obtained by introducing one additional matching point in each of the two GTD regions. Matching at $(x_d,0)$ on the x-wall gives

$$(33)\qquad \sum_{m=1}^{N} \alpha_m \ell_{nm} + D_h L_n\left(\frac{e^{-jkh}}{\sqrt{h}}\right) + \frac{1}{2}\, D_x \frac{e^{-jkx_d}}{\sqrt{x_d}}$$

$$= -H_z^i(x_d,0) - \frac{1}{2}\,(J_x^i+J_x^r)_{x=x_d} - L_n(J_h^i+J_h^r)$$

Similarly, matching on the h-wall gives

$$(34)\qquad \sum_{m=1}^{N} \alpha_m \ell_{mn} + \frac{1}{2}\, D_h \frac{e^{-jkh_d}}{\sqrt{h_d}} + D_x L_n\left(\frac{e^{-jkx}}{\sqrt{x}}\right)$$

$$= -H_z^i(h=h_d) - \frac{1}{2}\,(J_h^i+J_h^r)_{h=h_d} - L_n(J_x^i+J_x^r)\ .$$

Now we have N+2 equations to solve for N+2 unknowns. This system of simultaneous linear equations can be easily solved by the numerical matrix inversion technique.

The integrations over the GTD region are infinite in theory; however, in practice, one can approximately carry out the integration over a finite region because the Hankel function causes the integrand to become negligible for large value of ρ'.

The above approach is valid except near the shadow boundaries. In order to solve for the diffracted currents on or near a shadow boundary one should represent the diffracted currents in terms of an infinite series as given by [28]

$$J^d = \sum_{\ell=0}^{\infty} C_\ell \frac{e^{-jk\ell}}{(\sqrt{\rho})^\ell}\ .$$

However, in practice, if the currents are analyzed directly along a shadow boundary, then the diffracted current can be simply expressed by [28]

$$J^d = C_0\, e^{-jk\rho}\ .$$

The hybrid method gives good results for finite bodies. But it fails to determine the diffracted field of an infinite structure accurately. The values of D_h and D_x are found to be sensitive with respect to the position of the GTD matching points in the case of infinite geometries. This appraoch also requires extensive numerical integration to evaluate the coefficients $L_n(J^{GTD})$ and the excitation g_n' of the matrix equation.

C. A Modified Hybrid Method

The key to the modified hybrid method is to separate the total surface current of the impedance-loaded wedge into two components, namely: the current for the perfectly conducting case, J_c: and the change in current due to the presence of the surface impedance, ΔJ. Substituting $J = J_c + \Delta J$ into Eq. (22) gives

$$(35)\quad -H_z^i(s') = \frac{1}{2} J_c(s') + \frac{k}{4}\int_s \frac{Z_s}{\eta_o} J_c(s)\, H_o^{(2)}(k|\vec{\rho}'-\vec{\rho}|)ds$$

$$+ \frac{jk}{4}\int_s J_c(s)\, \frac{(\vec{\rho}'-\vec{\rho})\cdot\hat{n}}{|\vec{\rho}'-\vec{\rho}|}\, H_1^{(2)}(k|\vec{\rho}'-\vec{\rho}|)ds$$

$$+ \frac{1}{2}\Delta J(s') + \frac{k}{4}\int_s \frac{Z_s}{\eta_o}\Delta J(s)\, H_o^{(2)}(k|\vec{\rho}'-\vec{\rho}|)ds$$

$$+ \frac{jk}{4}\int_s \Delta J(s)\, \frac{(\vec{\rho}'-\vec{\rho})\cdot\hat{n}}{|\vec{\rho}'-\vec{\rho}|}\, H_1^{(2)}(k|\vec{\rho}'-\vec{\rho}|)ds\ .$$

Since J_c satisfies the special case, $Z_s=0$, of the integral equation, i.e.,

$$(36)\qquad H_z^i(s') = \frac{1}{2} J_c(s') + \frac{jk}{4}\int_s J_c(s)\, \frac{(\vec{\rho}'-\vec{\rho})\cdot\hat{n}}{|\vec{\rho}'-\vec{\rho}|}\, H_1^{(2)}(k|\vec{\rho}'-\vec{\rho}|)ds$$

Eq. (35) reduces to

$$(37)\quad -\frac{k}{4}\int_s \frac{Z_s}{\eta_0} J_c(s) H_0^{(2)}(k|\vec{\rho}'-\vec{\rho}|)ds = \frac{1}{2}\Delta J(s')$$

$$+\frac{k}{4}\int_s \frac{Z_s}{\eta_0}\Delta J(s) H_0^{(2)}(k|\vec{\rho}'-\vec{\rho}|)ds + \frac{jk}{4}\int_s \Delta J(s)\frac{(\vec{\rho}'-\vec{\rho})\cdot\hat{n}}{|\vec{\rho}'-\vec{\rho}|}$$

$$\cdot H_1^{(2)}(k|\vec{\rho}'-\vec{\rho}|)ds .$$

Define the change in surface current density as

$$\Delta J = \begin{cases} \Delta J^{GTD} & h_c \le h \le \infty \quad \text{on h-wall} \\ \Delta J^{MM} & 0 \le h \le h_c \quad \text{on h-wall} \\ \Delta J^{GTD} & x_c \le x \le \infty \quad \text{on x-wall} \\ \Delta J^{MM} & 0 \le x \le x_c \quad \text{on x-wall} \end{cases}$$

where ΔJ^{GTD} has the form of $\Delta D\ (e^{-jk\rho})/\sqrt{\rho}$, and the moment method incremental current can be expressed in terms of simple orthogonal pulse function, such as

$$\Delta J^{MM} = \sum_{m=1}^{N} \Delta\alpha_m P_m(s-s_m) .$$

By point matching at the center of each pulse, one obtains

$$(38)\quad \sum_{m=1}^{N} \Delta\alpha_m \ell_{mn} + \Delta D_x L_n\left(\frac{e^{-jkx}}{\sqrt{x}}\right) + \Delta D_h L_n\left(\frac{e^{-jkh}}{\sqrt{h}}\right) = g_n \quad 1 \le n \le N$$

where ℓ_{mn} and L_n are the same as in section B and

$$(39)\quad g_n = -\frac{k}{4}\int_s \frac{Z_s}{\eta_0} J_c(s) H_0^{(2)}(k|\vec{\rho}'-\vec{\rho}|)ds .$$

Again, two additional equations will be obtained from the matching in the GTD regions. A system of N+2 simultaneous linear equations will be solved for $\Delta\alpha_m$'s and ΔD_x, ΔD_h, by numerical matrix inversion technique.

It should be noted that two of the integrals in Eq. (37) are limited to only the contour where Z_s is non-vanishing. Consequently, for conducting scatterers with small inhomogenities with $Z_s \neq 0$ those two integrals can be readily and accurately evaluated. Furthermore, as a consequence of separating the current J_c for the perfectly conducting body, the geometrical optics currents are not included in the third integral of Eq. (37) which involves ΔJ. Thus the third integral converges rapidly because only diffracted components are included in ΔJ. Those features of the ΔJ approach result not only in significantly improved efficiency, but also provide reasonable accuracy for the diffracted fields. Computer solutions of the integral equations typically result in accuracies of a few percent. Thus ΔJ and the resulting diffracted current can be calculated to within a few percent. However, the original hybrid method of Eq. (22) yields the same accuracy for the total current. This results in very poor accuracy for the diffracted component which is typically a small fraction of the total current. This "ΔJ" approach has then a distinct advantage if one wishes to isolate the diffraction of some isolated anomally in the presence of an edge.

CHAPTER IV

THE REDUCTION OF BACKSCATTERED FIELD --- TWO-DIMENSIONAL CASE

A. Introduction

Edge diffracted fields become a dominant contributor to the scattered fields for a wide variety of geometries. These usually are significant when the observation point is not illuminated by a specular field. Some examples include: the cone for near axial incidence, the leading or trailing edge of a wing for sufficiently low frequencies. These fields are generally considered to be low but this is only when considered with respect to the specular contribution from a surface.

It is the goal of this study to achieve further reduction of back scattered fields from the edge diffraction mechanism over reasonable range of incidence angles and broad frequency band by use of antenna impedance loading. Absorbing material was often used in the study of backscatter reduction. However, it is usually necessary to cover a substantial part of the body of an aircraft or space craft. The presence of a large absorber could seriously affect the performance of the aircraft. This is not desirable because it would require the redesign of the whole aircraft structure. In this chapter, the possibility of designing an antenna to scatter energy at least in some direction or range of directions in such a way to cancel or reduce the edge diffracted field in that range of direction is considered. Surface impedance is used to model slot antenna. The hybrid methods discussed in Chapter III are employed to treat various geometries and the results for optimum loading are also presented.

B. The Triangular Cylinder

The reaction integral equation and the Galerkin's method with a piece-wise sinusoidal basis, developed by Richmond [30], is used to study the scattering by a two-dimensional, triangular wedge-shaped cylinder. The scattering geometry of a triangular cylinder is quite suitable for providing information on the effectiveness of impedance loading for backscatter reduction. Furthermore, this geometry provides efficient numerical results. Results on optimum loading configurations obtained from this geometry will be directly applicable to a wide variety of scattering geometries such as conical shapes and ogive shape or similar wing structures.

In order to isolate the effect of the impedance loading a source excitation is being used that consists of two line sources located on the cylinder surface and phased to null out the effect of the other edge. The wedge-shaped cylinder without impedance loading can readily

be analyzed by the GTD or wedge diffraction approach. The wedge diffraction analysis for the unloaded cylinder was programmed as a check case. The value of the wedge diffraction check was demonstrated when it revealed an insufficient number of piece-wise sinusoidal monopoles were used in the reaction integral equation program. The results obtained by using 4 segments in one wavelength and the GTD results are shown in Fig. 6. The difference between these two results is significant. However, if 8 segments in one wavelength are used, the result agrees well with the GTD result (see Fig. 7).

Due to limitations on the dimensions of the wedge cylinder that can practically be used in the reaction integral equation program on the DATACRAFT 6024 computer, results can only be obtained for cylinders on the order of 2.5λ or smaller in width. However, several promising results have been obtained using the integral equation program. These results indicate that considerable reduction can be achieved in the backscattering from the edge diffraction mechanism. In one case a reduction of 14 dB was obtained using a real impedance loading of 377 ohms located right at the edge as shown in Fig. 8. The computed results also show that similar reduction can be achieved by a reactive loading of Z_s = -j188 ohms located 5/8λ from the edge, as shown in Fig. 9.

The backscattered fields of such a wedge geometry have also been computed as a function of incidence angle and surface impedance. This analysis shows the reduction of the edge diffracted field discussed above is maintained from angles of zero (preceding case) to about 60° when the surface impedance is at the edge. Figure 10 shows the backscattered fields with zero and 188 ohms surface impedance. Note that the lobes are decreased from 40°-100°. For plane wave incidence as shown in Fig. 10 the effect of the edge that does not have impedance loading cannot be isolated from the edge with loading. Consequently, the reduction in backscatter as shown in Fig. 10 represents a considerable reduction achieved by the loaded edge. This corresponds to the reduction achieved in Fig. 8, but also demonstrates the wide angle coverage that can be achieved. Thus, the above analysis does indicate that the desired control can be achieved.

C. The Infinite Wedge

The hybrid methods discussed in Chapter II were programmed for the analysis of the infinite wedge with impedance loading. The total current on a perfectly conducting wedge surface was calculated by the hybrid method of Eq. (22). The current was sampled using a 0.1λ or smaller spacing between sampling points in the MM region. The moment method region is 1λ in length and each GTD matching point is 1.25λ away from the edge tip. Results for the surface current density and the diffracted field of a 30° conducting wedge with plane wave incidence are compared with GTD, as shown in Figs. 11-12. Although the original hybrid method was found to yield reasonable results for the

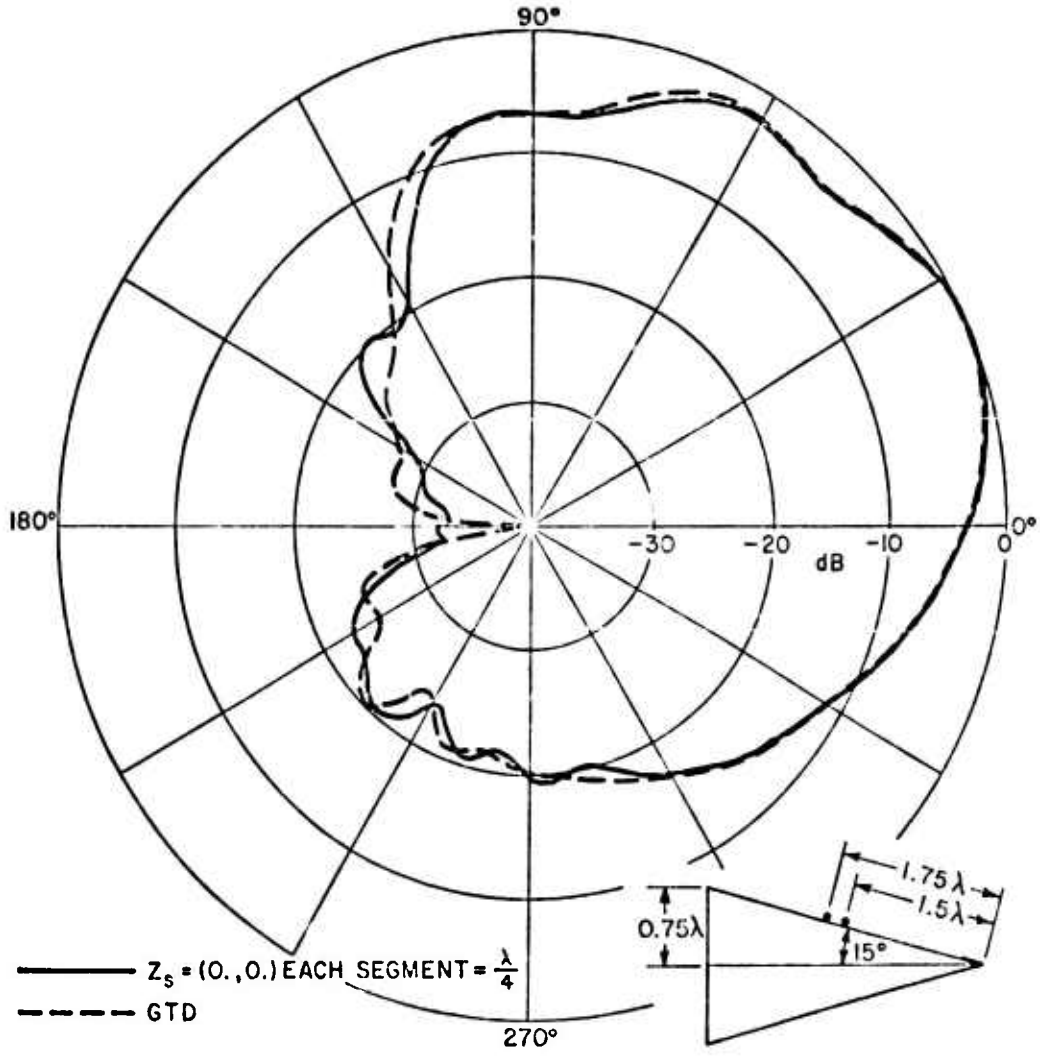

Fig. 6--Comparison of patterns from GTD and integral equation solution.

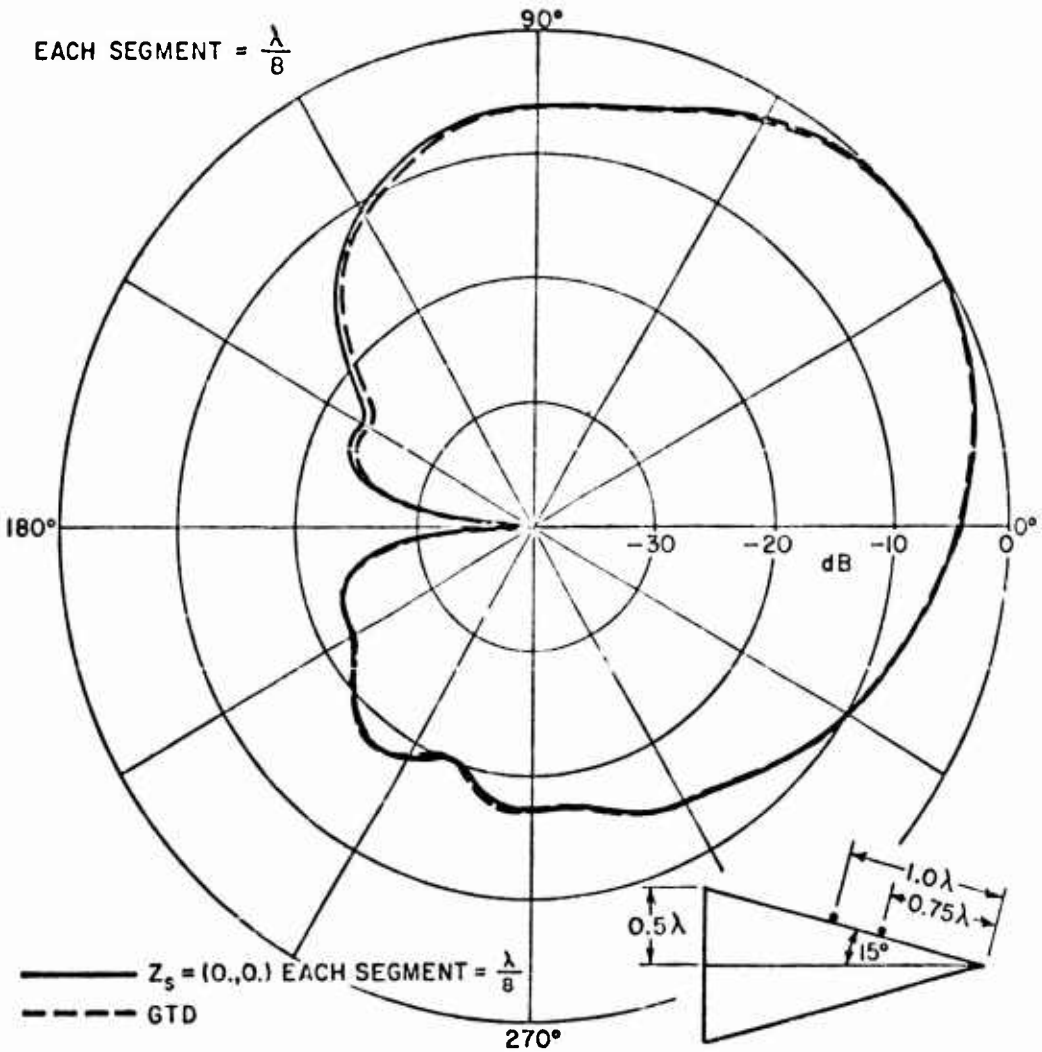

Fig. 7--Comparison of patterns from GTD and integral equation solution.

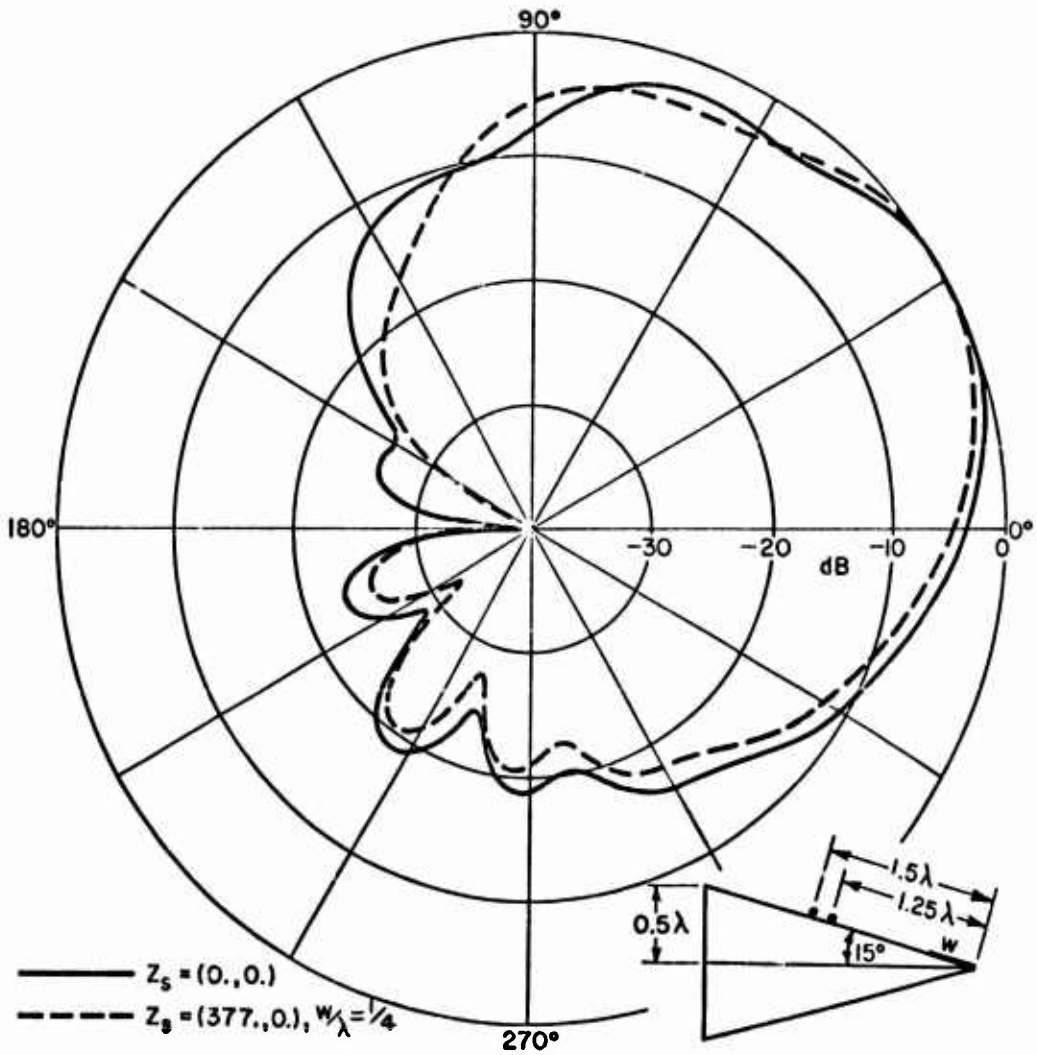

Fig. 8--Comparison of radiation patterns with and without surface impedance.

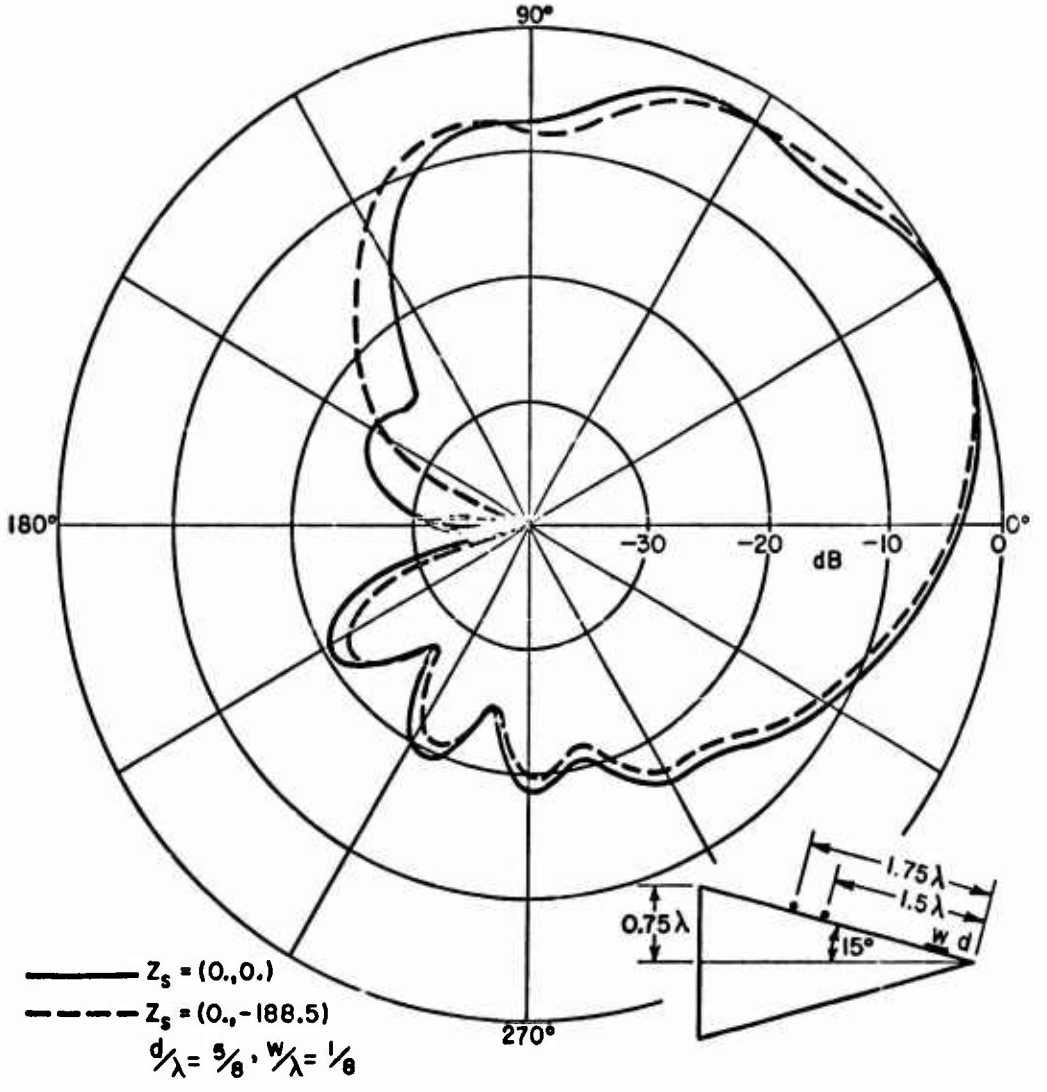

Fig. 9--Comparison of radiation patterns with and without surface impedance.

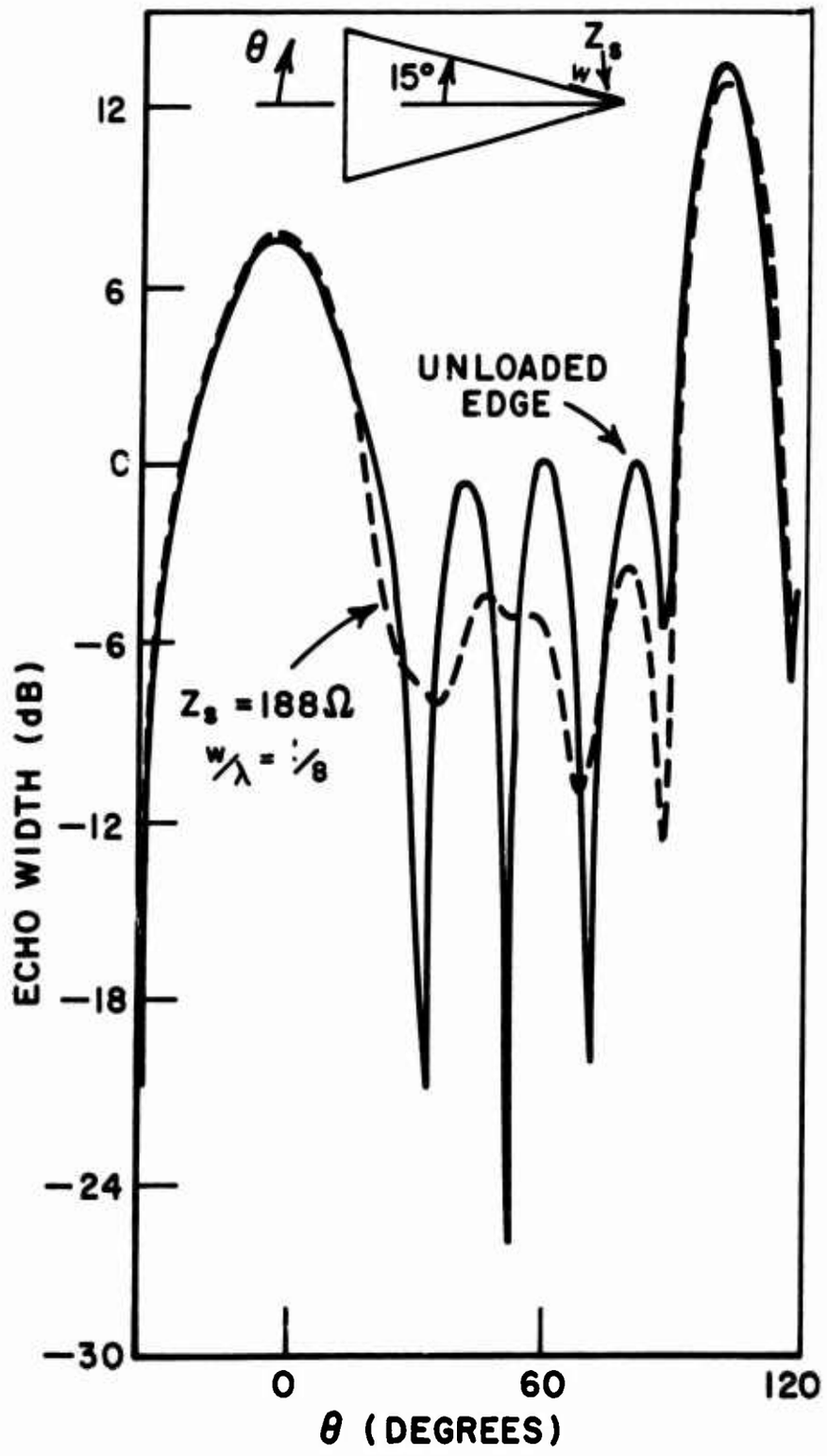

Fig. 10--Plane wave backscatter from loaded and unloaded triangular cylinder.

total current and high-level fields of the scatterer, it fails to accurately predict low-level fields such as diffracted fields, as seen in Figs. 11-12. Consequently, the original hybrid method was found to be inadequate to analyze the performance of impedance techniques. After some research it was found that the original hybrid method could be extended to provide accurate results for low level diffracted fields.

As has been noted the key to the modified hybrid method is to seperate the surface current of an impedance loaded scatterer into two components: the current J_c for the perfectly conducting scatterer and the change in current ΔJ due to impedance loading. Since the current J_c for the perfectly conducting wedge is known, the current ΔJ on an impedance loaded wedge can be solved using the modified hybrid method. The current ΔJ is sampled using a 0.1λ or smaller spacing between sampling points in MM region. Since the current ΔJ decays rapidly away from any impedance loadings, the integrals of the modified method converge rapidly. This results in improved efficiency as well as accuracy compared to that of the original hybrid method.

The results of reduction in backscatter that can be achieved by impedance loading are shown in Figs. 13-18. A reduction of more than 15 dB is obtained in an angular range of 20° from grazing incidence for both 30° and 60° wedge. These reductions were also demonstrated at three different frequencies representative of a 3:1 frequency band. The impedance loading required over the continuous frequency range was also calculated. The required surface impedance loading over the 3:1 frequency range and the reduction in backscatter from the 30° infinite wedge are given in Table I. The surface impedance is plotted on a Smith chart in Fig. 19.

D. The Square Cylinder

The accuracy of the modified hybrid method was checked against the integral equation or moment method solution for the 4λ square cylinder with impedance loading as shown in Fig. 20. This cylinder size is close to the limit possible with the pure moment method. The accuracy of the modified hybrid method was found to be better than 6% even for low level fields. The computed results of the two methods are so close that the difference can not be seen on Fig. 20.

The scattered field from a square cylinder is shown in Fig. 21. The results for this case were calculated by all three methods: the moment method, the modified hybrid method and the original hybrid method. It was found that the original hybrid method gives good results for the 4λ cylinder in contrast to the case of the infinite wedge. Thus it can be concluded that the original hybrid method is sufficiently accurate for finite size scatterers for which the integrations involved in the original hybrid method are not truncated.

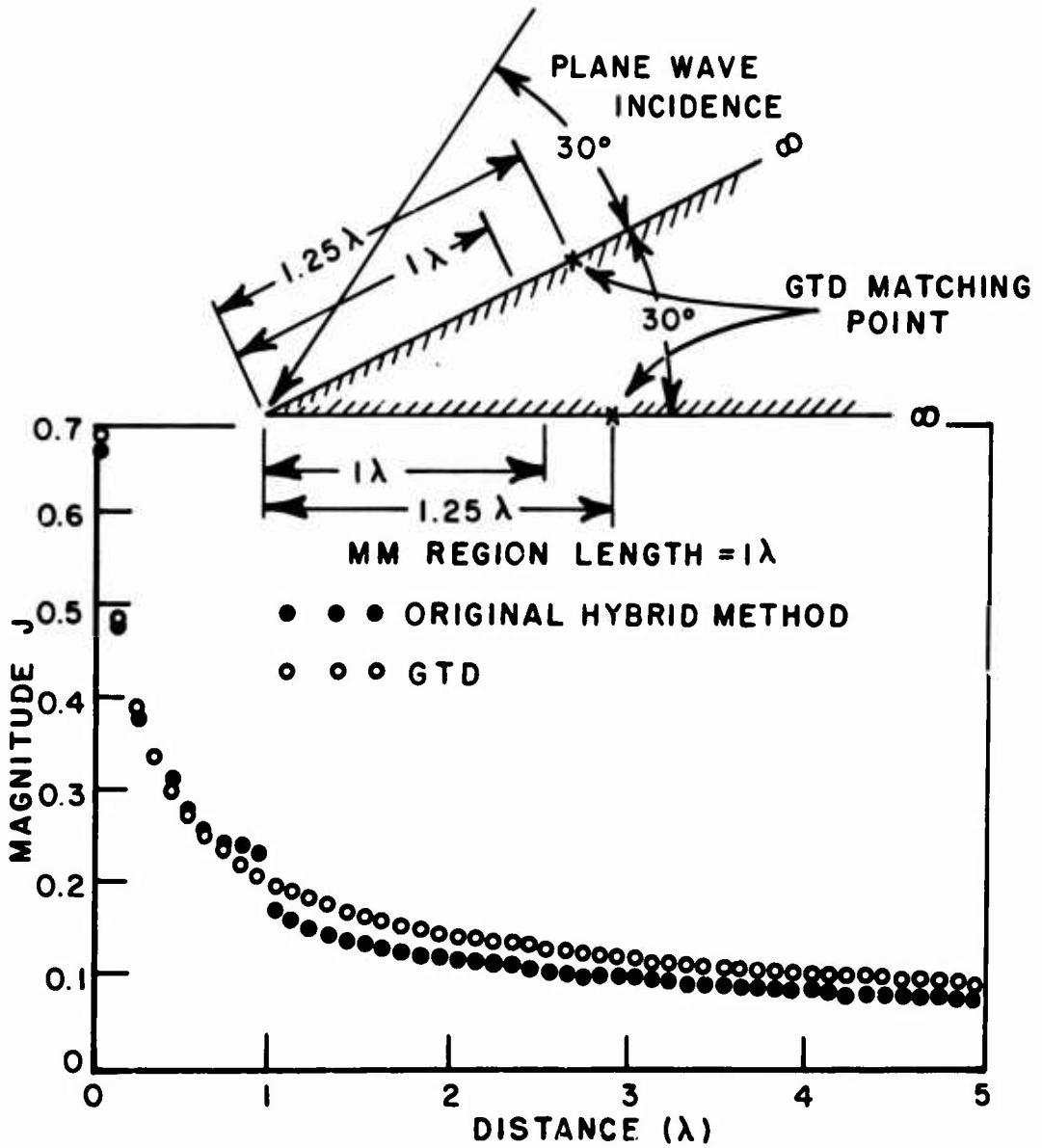

Fig. 11--Diffracted current on perfectly conducting wedge.

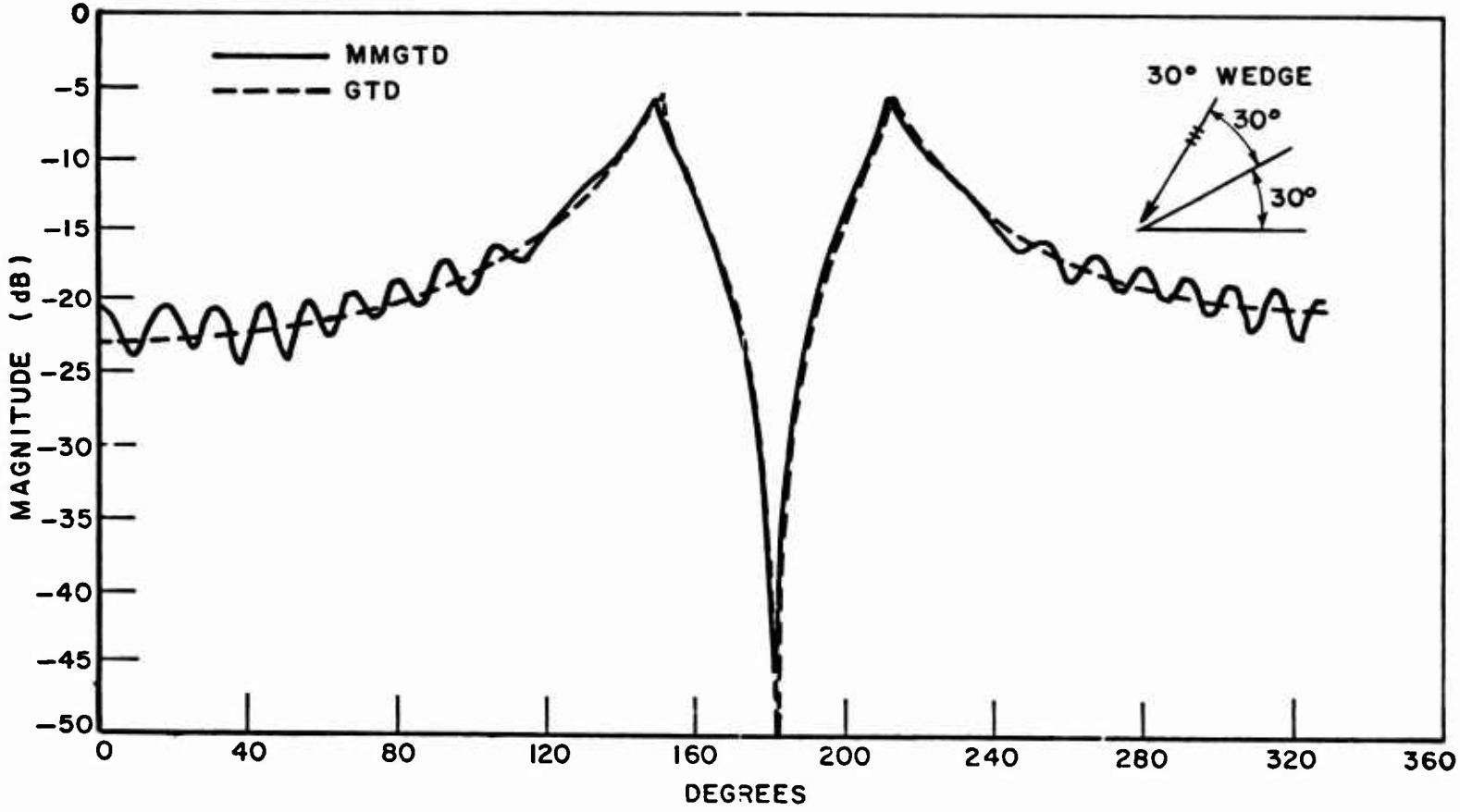

Fig. 12--Comparison of diffracted field by the original hybrid method and GTD.

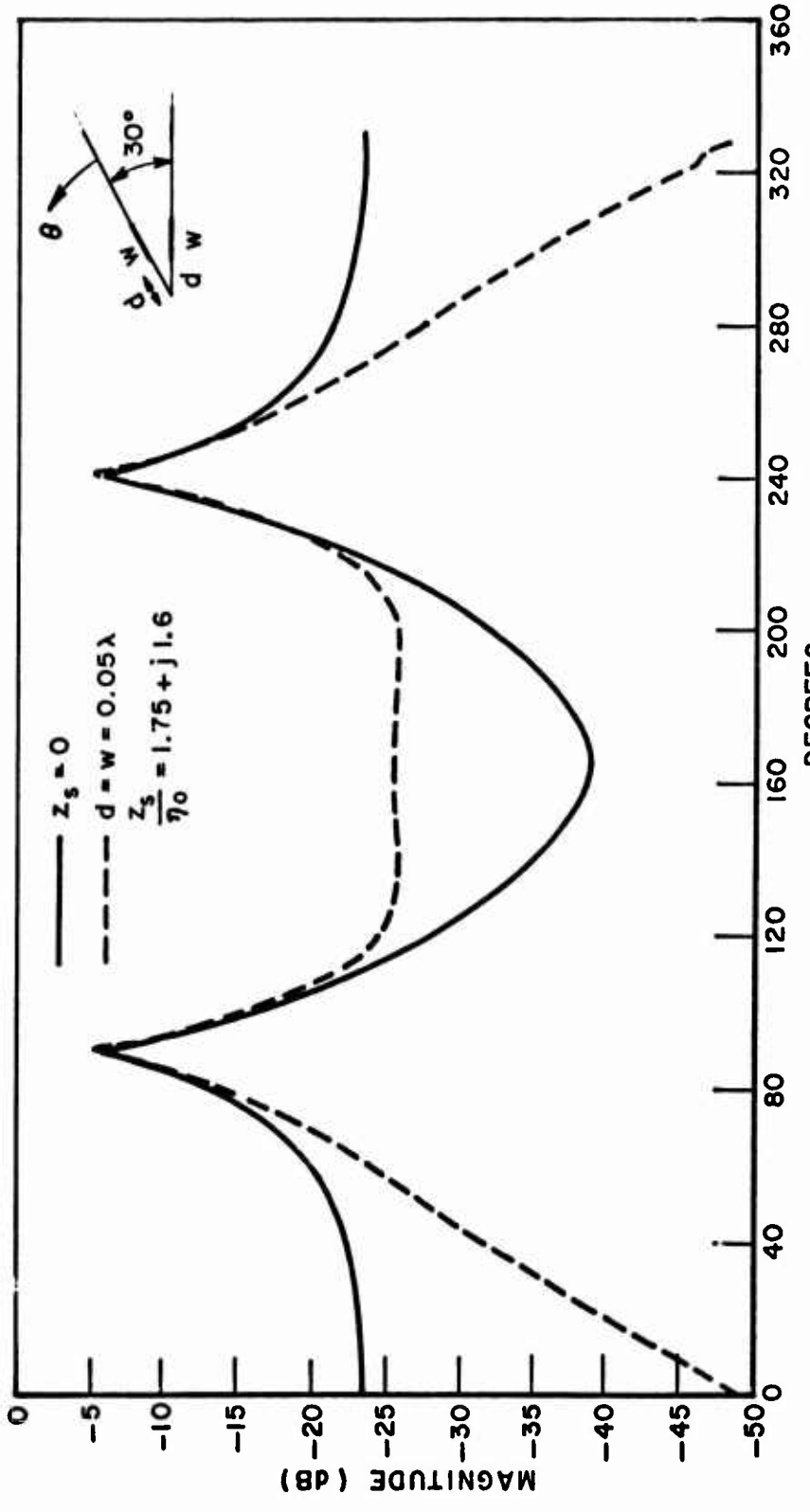

Fig. 13--Edge diffracted component of backscattered fields using surface impedance strips.

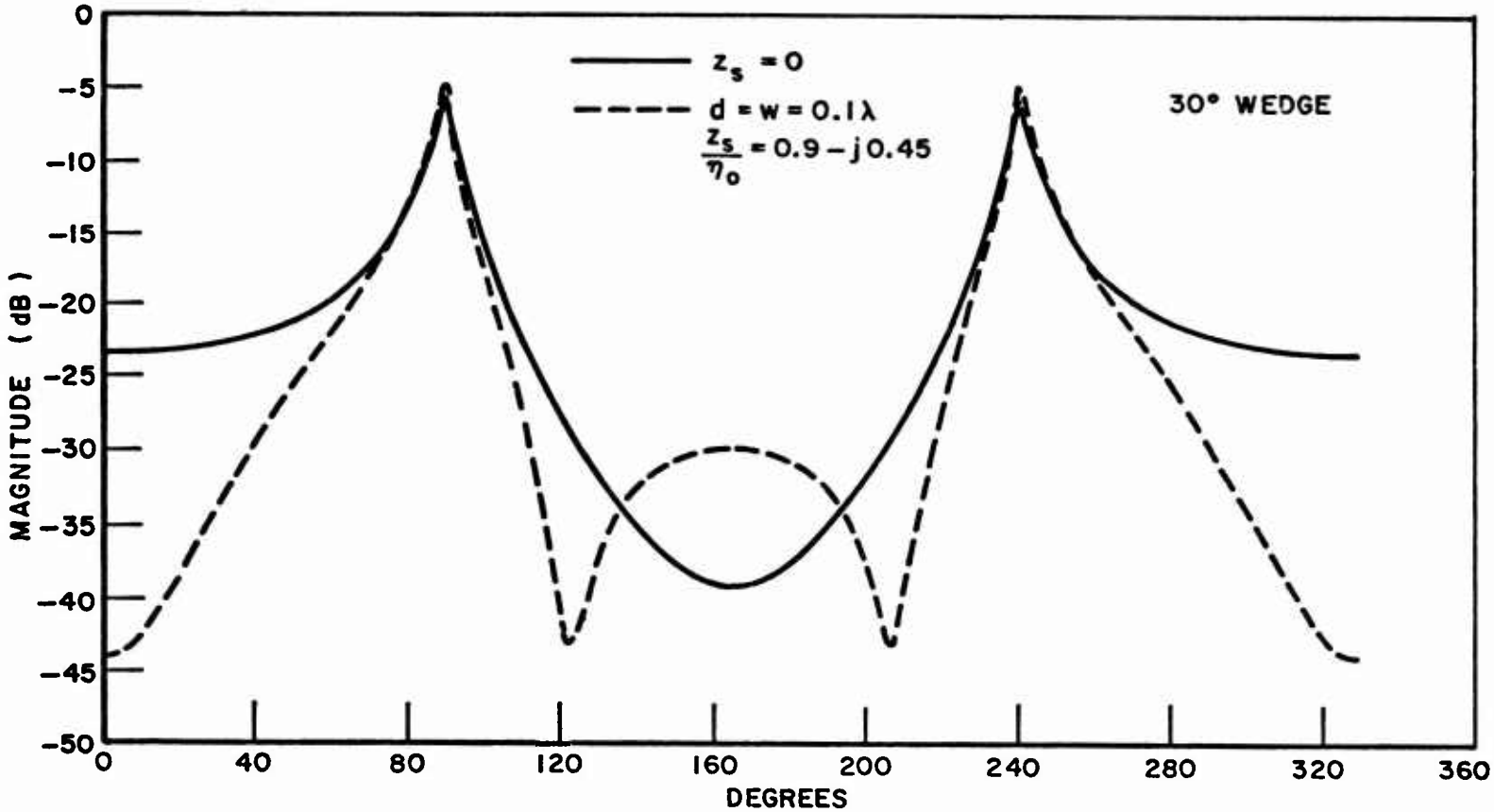

Fig. 14--Edge diffracted component of backscattered fields using surface impedance strips.

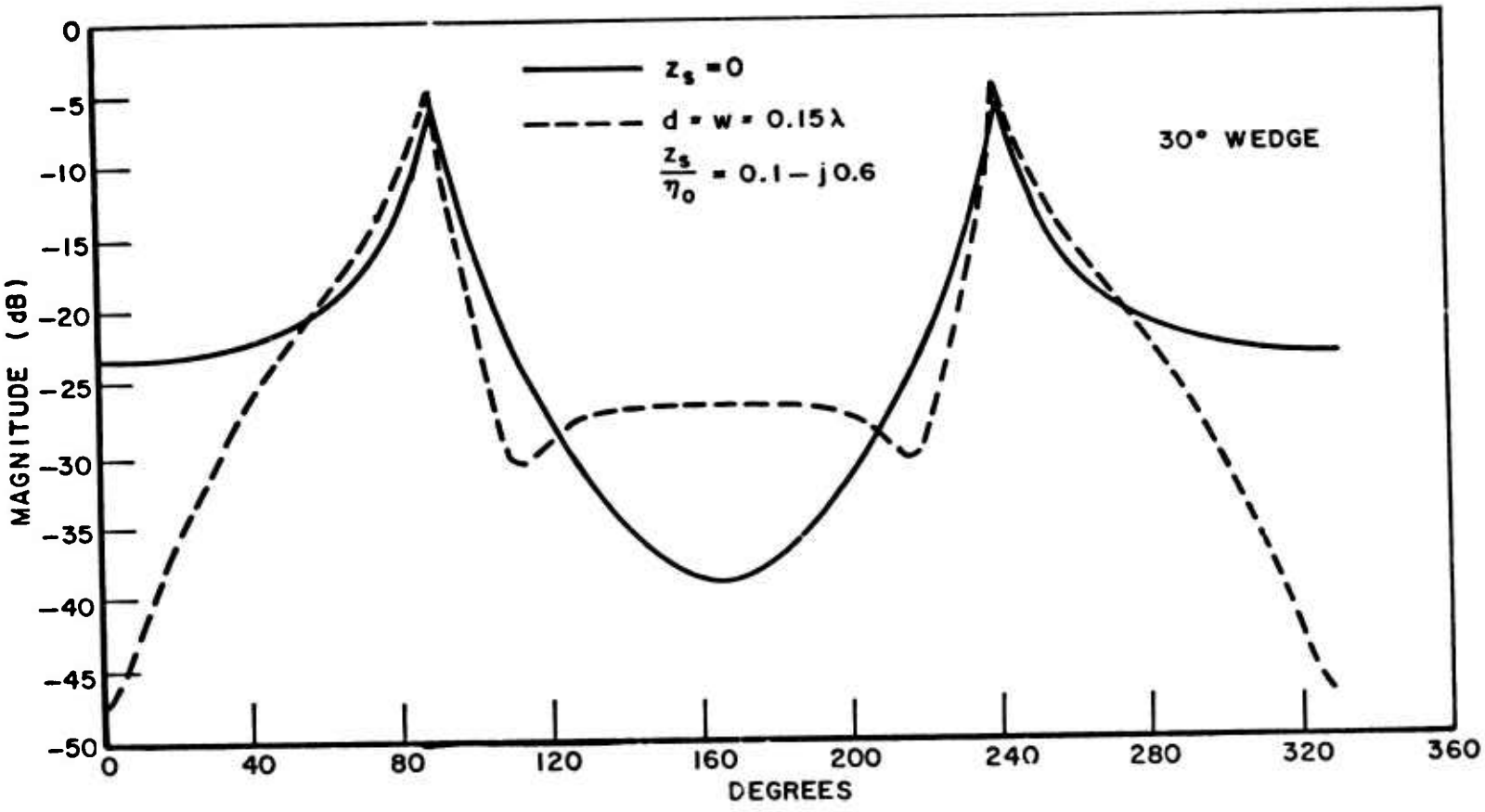

Fig. 15--Edge diffracted component of backscattered fields using surface impedance strips.

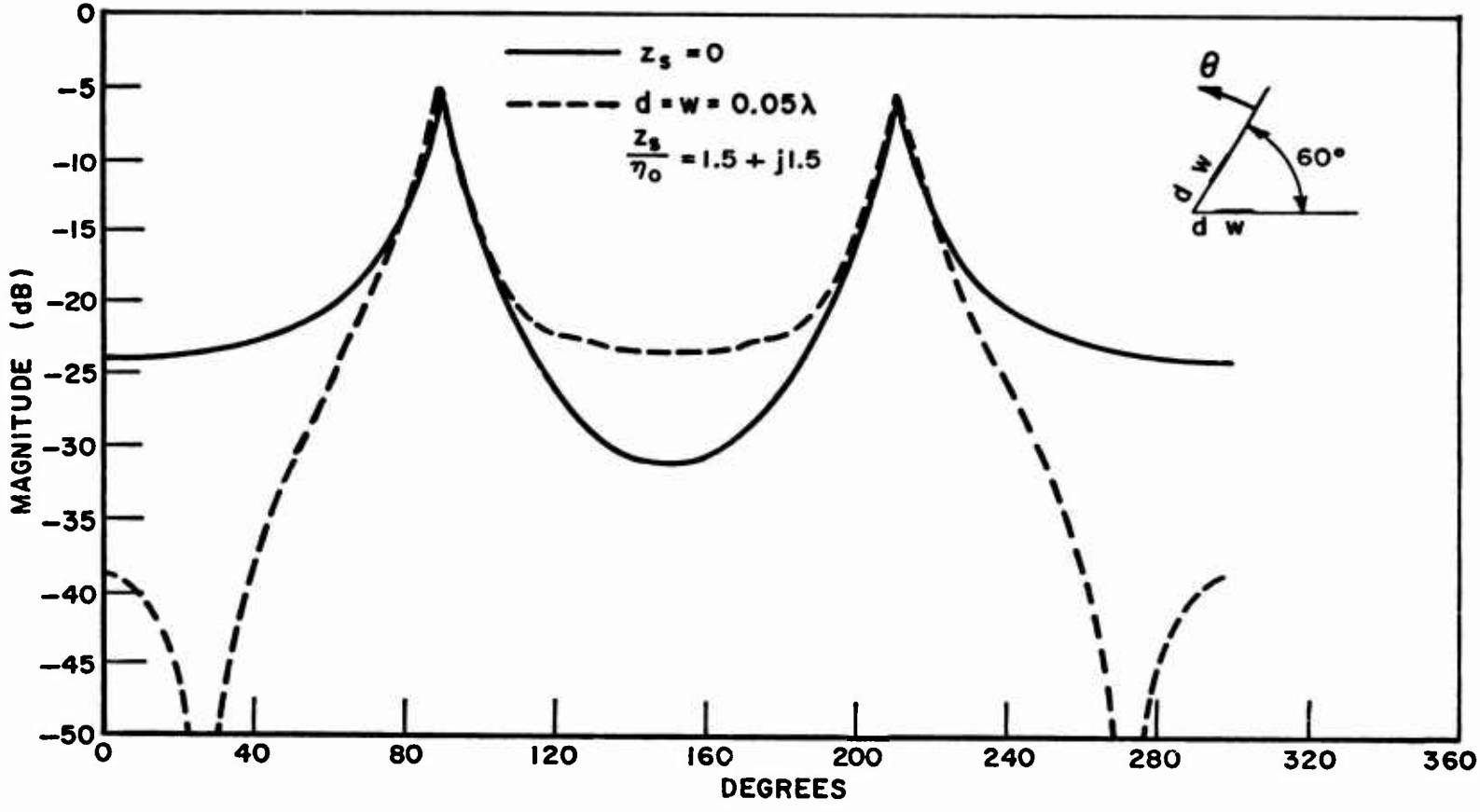

Fig. 16--Edge diffracted component of backscattered fields using surface impedance strips.

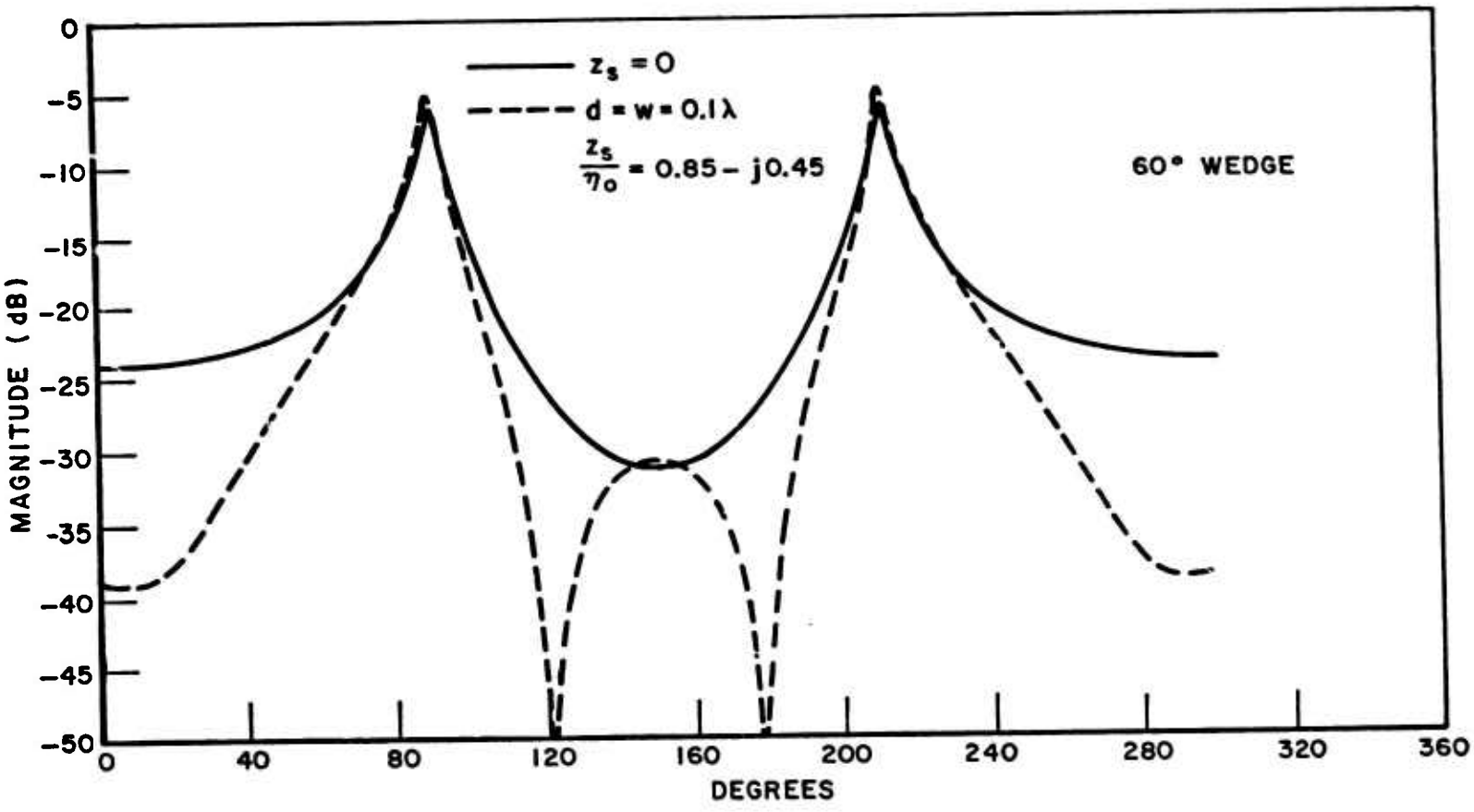

Fig. 17--Edge diffracted component of backscattered fields using surface impedance strips.

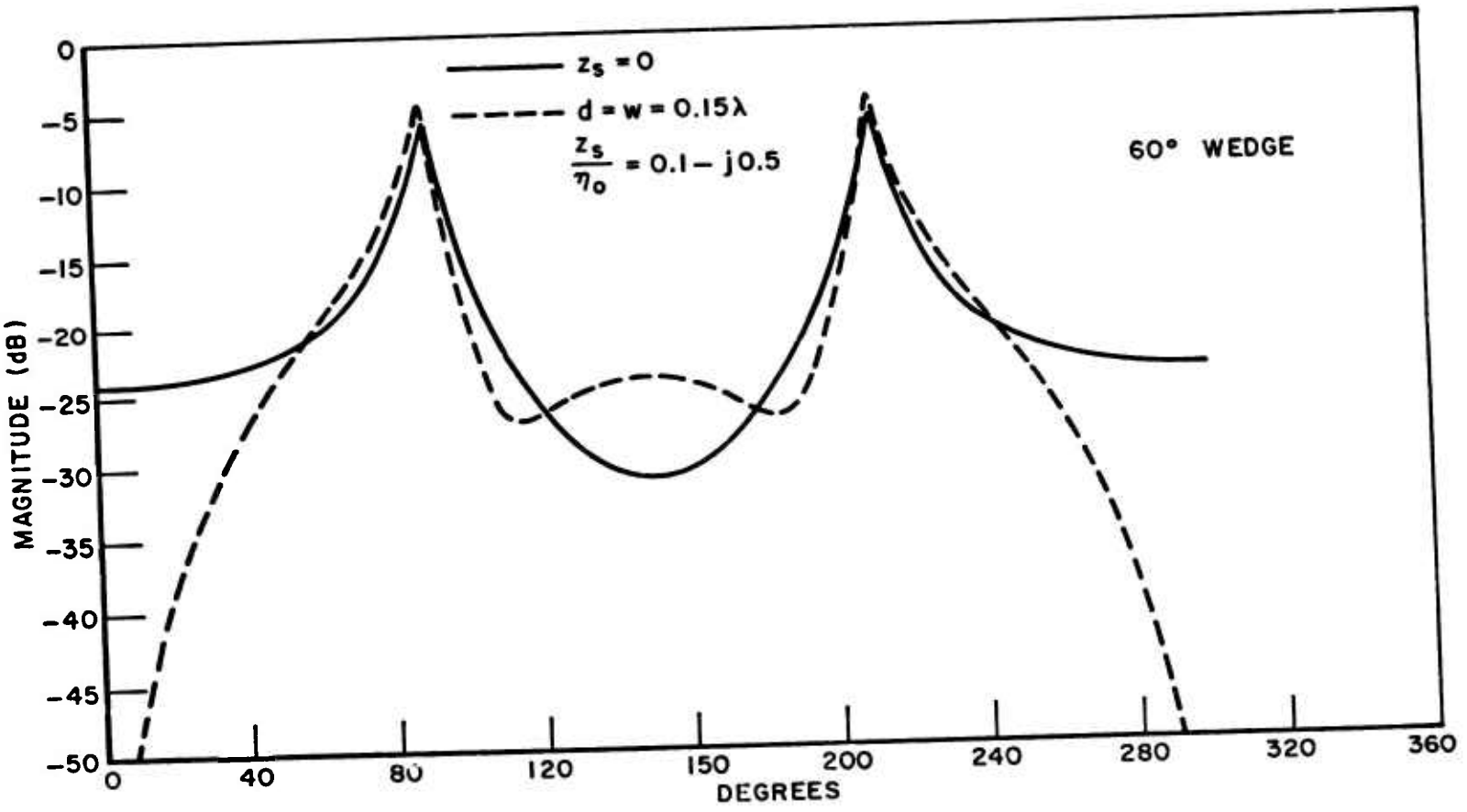

Fig. 18--Edge diffracted component of backscattered fields using surface impedance strips.

TABLE I

REDUCTION OF BACKSCATTER AT GRAZING INCIDENCE FOR 30° WEDGE

Z_s/η_o	d/λ	w/λ	Reduction (dB)
1.75+j1.6	0.05	0.05	25
1.85+j1.0	0.06	0.06	23
1.7 +j0.3	0.07	0.07	19.5
1.45-j0.1	0.08	0.08	18
1.15-j0.3	0.09	0.09	21
0.9 -j0.5	0.1	0.1	30
0.7 -j0.55	0.11	0.11	21.5
0.5 -j0.6	0.12	0.12	21
0.35-j0.6	0.13	0.13	23
0.23-j0.6	0.14	0.14	27
0.1 -j0.6	0.15	0.15	24

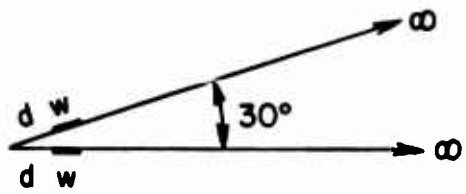

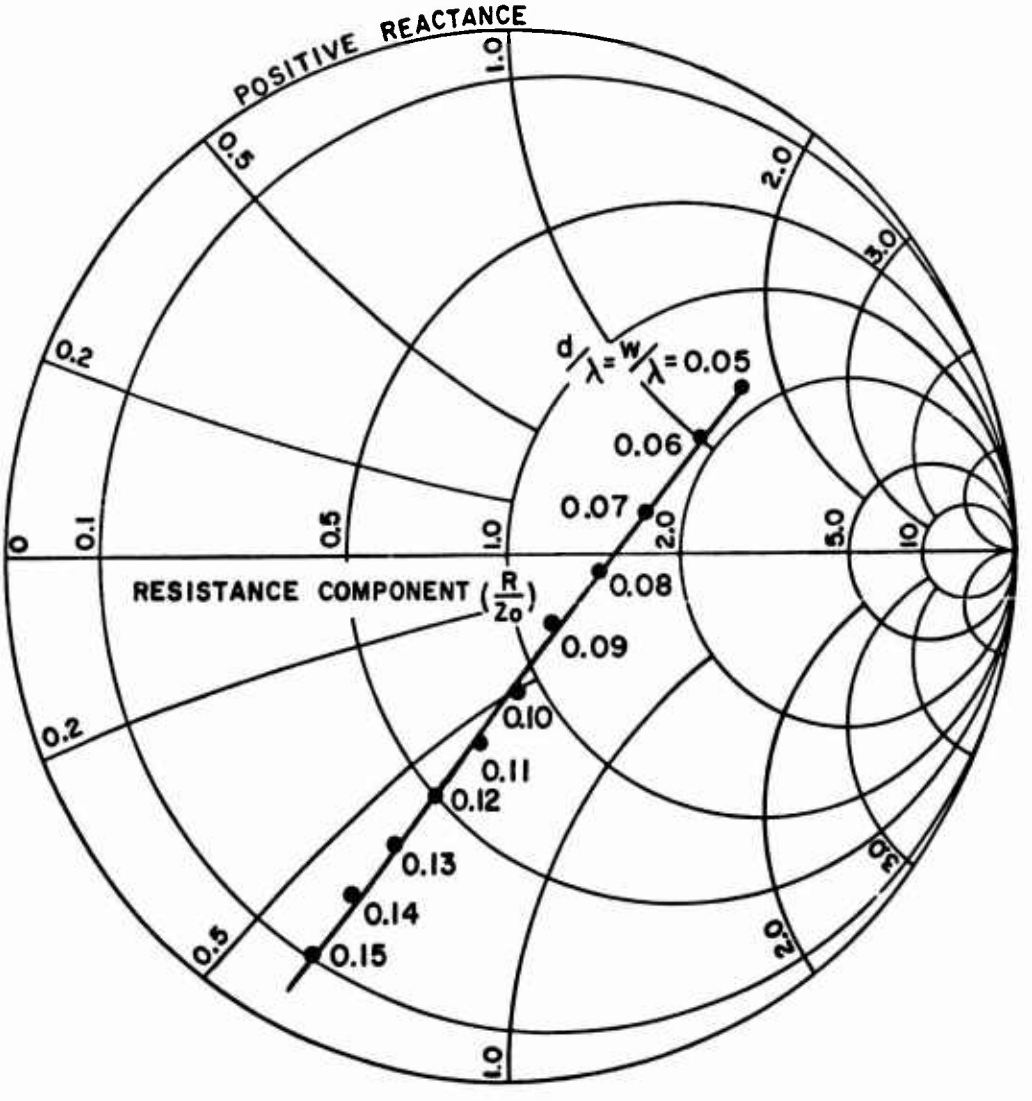

Fig. 19--Surface impedance to reduce backscatter from an infinite wedge over a 3:1 frequency band.

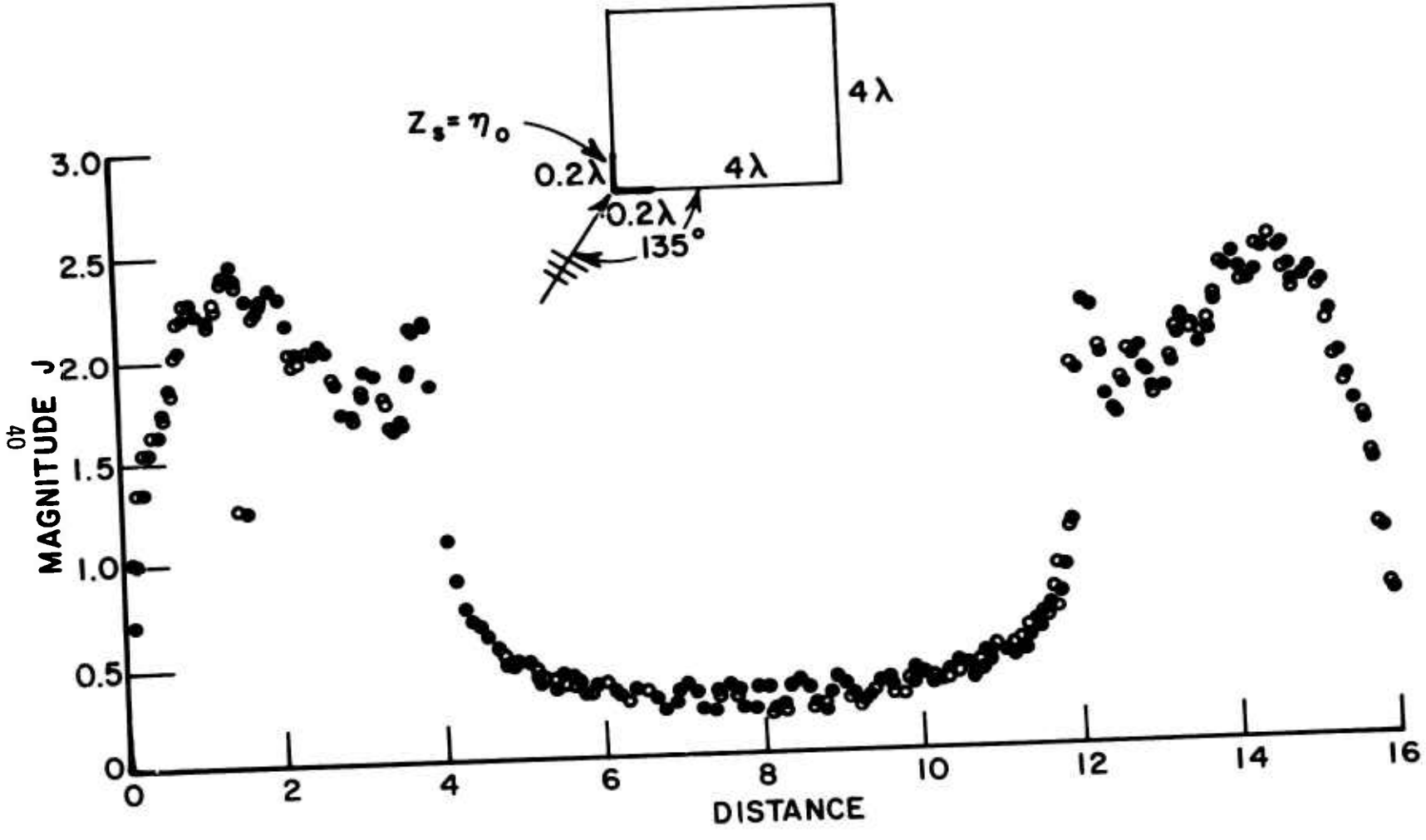

Fig. 20--Current on surface of conducting square cylinder with surface impedance loading.

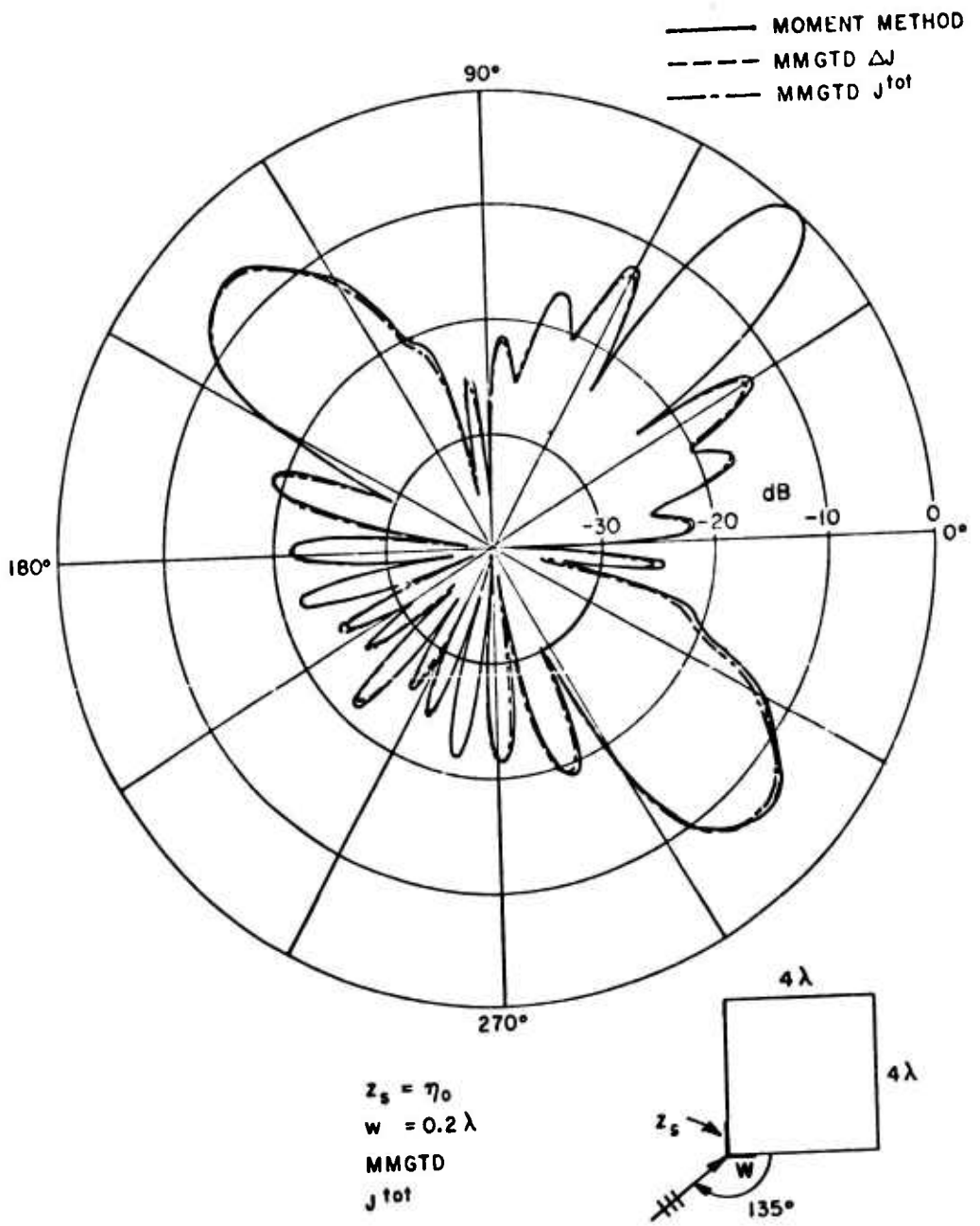

Fig. 21--Scattered field of conducting square cylinder with surface impedance loading.

E. A Two-dimensional Wing Model

The original hybrid method was used to analyze the two-dimensional wing model shown in Fig. 22(a). This wing model should provide a good simulation for a practical aircraft wing cross section. However, the small wedge (angle $\approx 6°$) of the wing model of Fig. 22(a) was found to cause a computational problem in the application of the hybrid method. After investigation of this problem it was discovered that the small wedge angle causes some of the matching points used in the point matching region around the edge to be too close for practical computation as shown in Fig. 22(b). This problem was overcome by truncation of the wedge tip as shown in Fig. 22(c). The truncation still permits a practical analysis of the edge loading because the trailing edge of the wing is very thin in wavelengths.

The current in the MM regions is again sampled using a 0.1λ or smaller spacing between sampling points. Since the primary interest is in the angular range which is close to grazing to the wedge arm, the diffracted currents from the wedge-cylinder junction are analyzed along or near the shadow boundary. The form $D_0 e^{-jk\ell} + D_1 (e^{-jk\ell})/\sqrt{\ell}$ is used for the diffracted currents from the wedge-cylinder junction, while $D (e^{-jkh})/\sqrt{h}$ is used for the diffracted currents from the wedge tip, as shown in Fig. 23.

The backscatter reduction of the two-dimensional wing model as a function of wing size and geometry, including the effect of the leading edge, has been investigated. The scattered fields for $Z_s = 0$ and $Z_s = \eta_0$ on the leading edge were checked by using the hybrid method and the moment method for $a = 0.075\lambda$, 0.1λ, 0.15λ, 0.2λ, 0.25λ and 0.3λ. Figures 24-25 show some of the typical checks. Tables II and III show the backscatter reduction from the leading and trailing edge for various wing size. The leading edge is dominant for wing radii greater than 0.1λ. However, the leading edge contribution can be reduced by more than 12 dB for $a \geq 0.2\lambda$, as shown in Fig. 26. This is achieved by covering the leading edge with a surface impedance $Z_s = \eta_0$. For wing radii smaller than 0.1λ, the trailing edge contribution is more important. By loading the trailing edge with a 0.1λ wide surface impedance, the backscatter for a thin wing can be reduced by 10.19 dB, as shown in Fig. 27. The backscatter reduction from the leading and trailing edge, respectively, as a function of incidence angle is also calculated and shown in Tables IV and V. It is seen from Fig. 28 that further reduction can be obtained if both edges are loaded. The reduction in Fig. 28 is 11.33 dB, compared to 5.79 dB when only the leading edge is loaded and 5.37 dB when only the trailing edge is loaded.

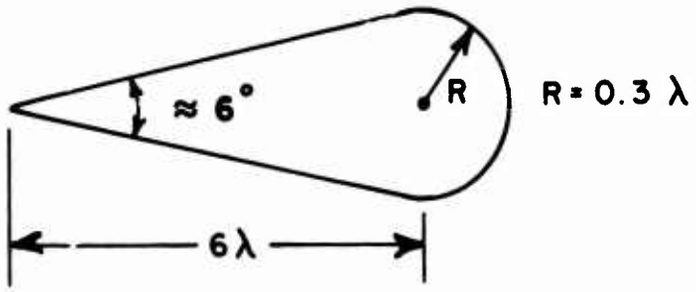

(a)

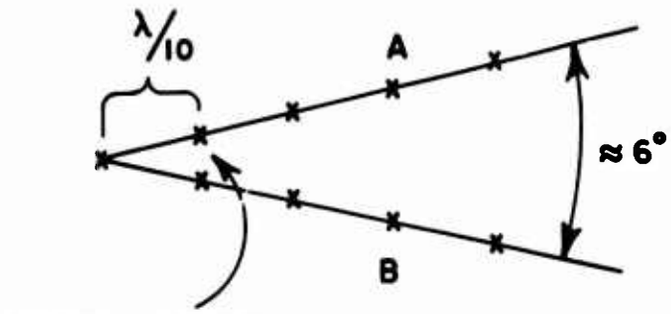

(b)

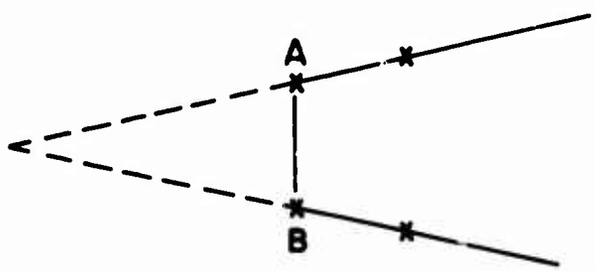

(c)

Fig. 22--Point-matching problem for small-angle wedge.

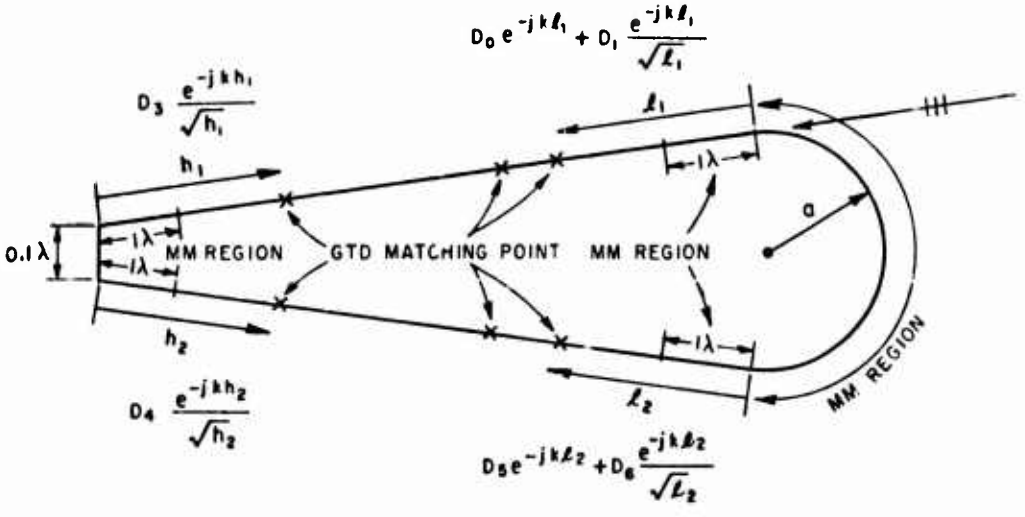

Fig. 23--MMGTD method applied to the two-dimensional wing model.

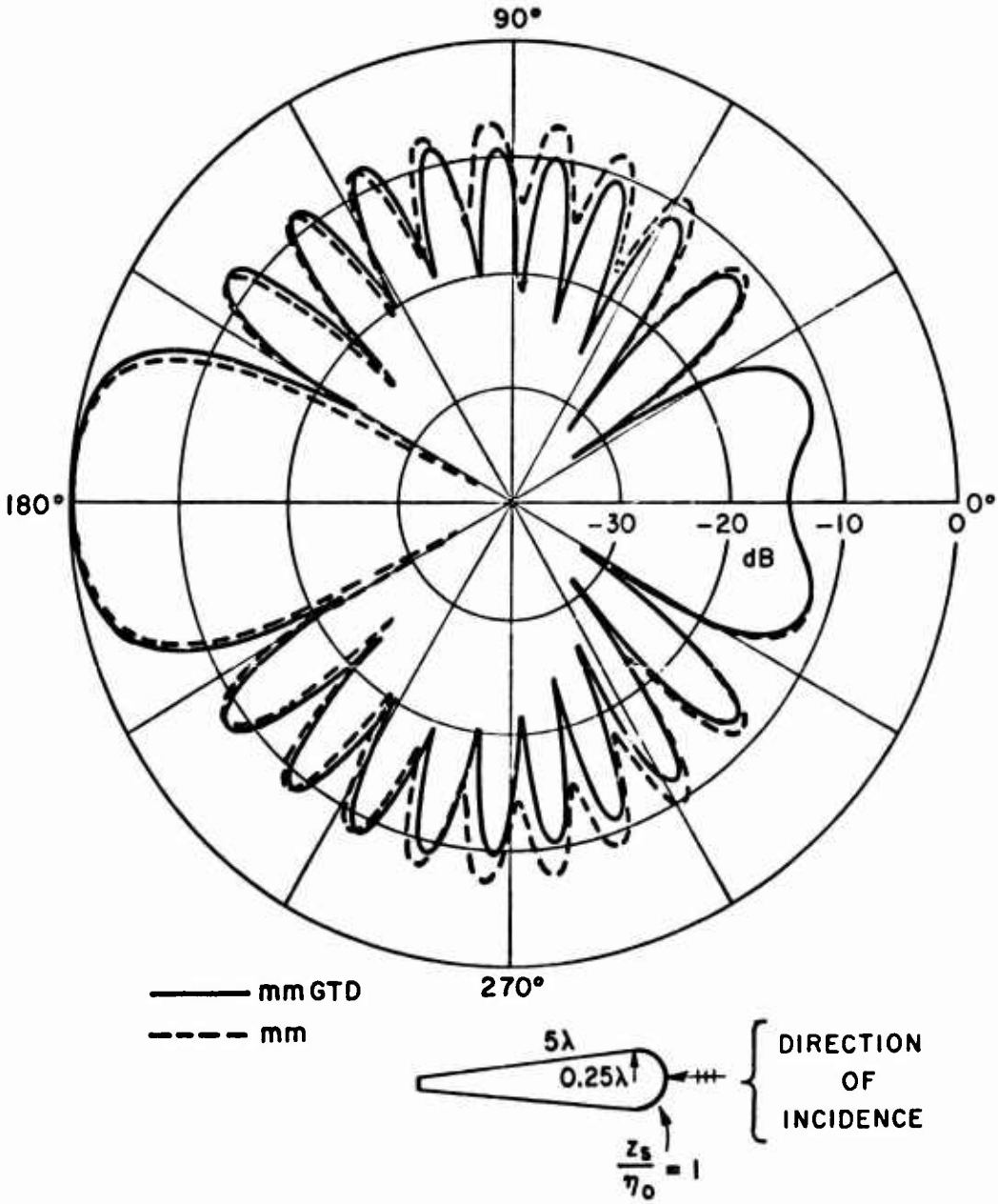

Fig. 24--Comparison of bistatic scattered fields obtained using MM and MMGTD solutions for a wing foil with impedance loading.

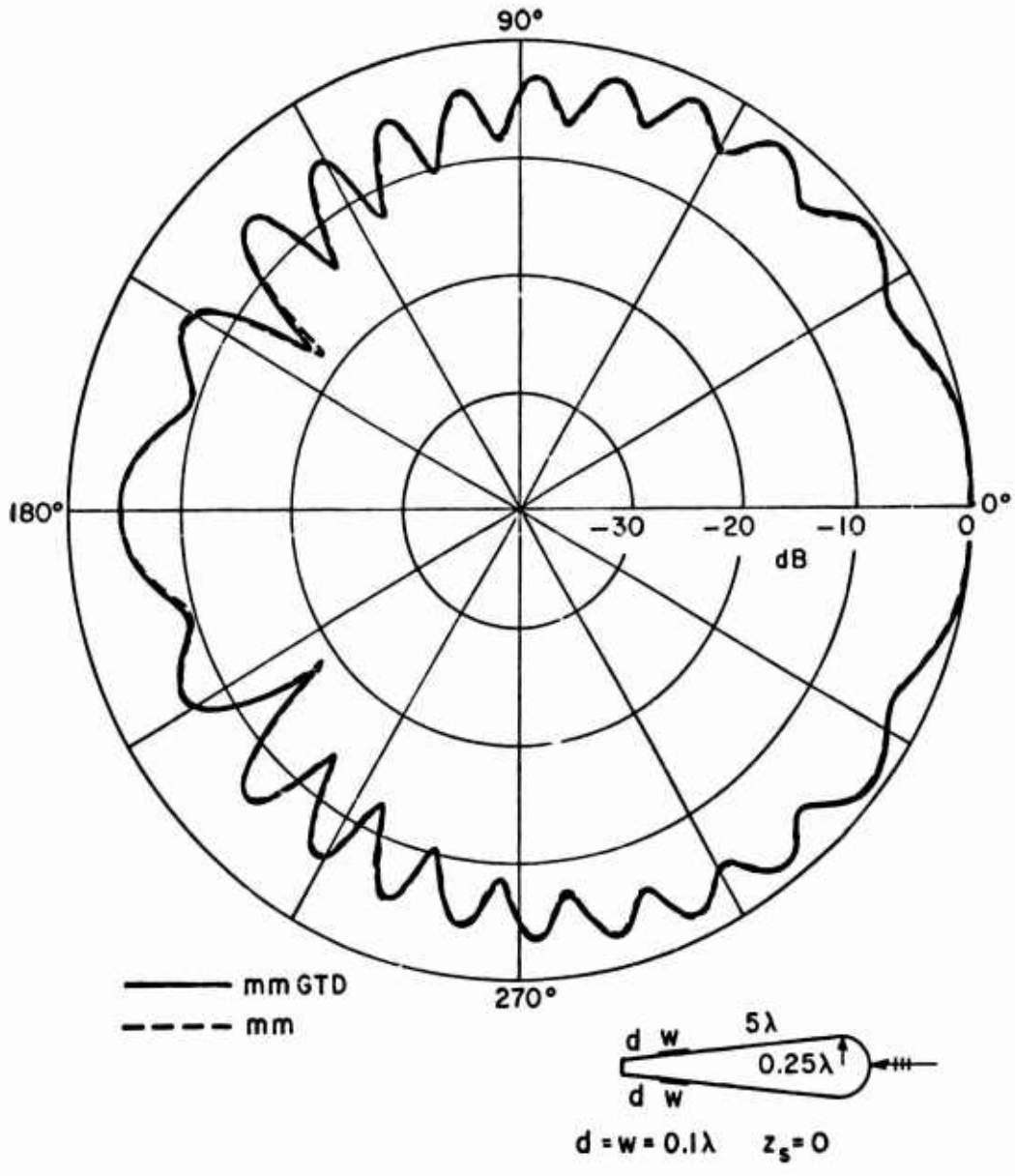

Fig. 25--Comparison of bistatic scattered feilds obtained using MM and MMGTD solutions for a wing foil with impedance loading.

TABLE II

BACKSCATTER REDUCTION BY LOADING THE LEADING EDGE

Radius (a)	Backscatter Reduction (dB) Moment Method	MMGTD
0.3λ	17.77	18.00
0.25λ	14.89	14.92
0.2λ	12.28	12.24
0.15λ	9.42	9.40
0.1λ	5.85	5.79
0.075λ	3.30	3.30

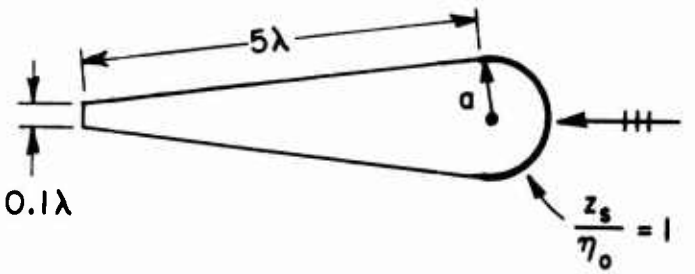

TABLE III

BACKSCATTER REDUCTION BY LOADING THE TRAILING EDGE

Radius (a)	Backscatter Reduction (dB)
0.3λ	-1.0
0.25λ	0.05
0.20λ	1.29
0.15λ	2.06
0.10λ	5.37
0.075λ	10.19

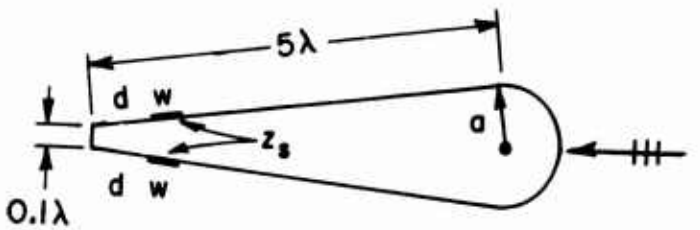

$d = w = 0.1\lambda$

$\frac{z_s}{\eta_0} = 1.0 - j \cdot 0.6$

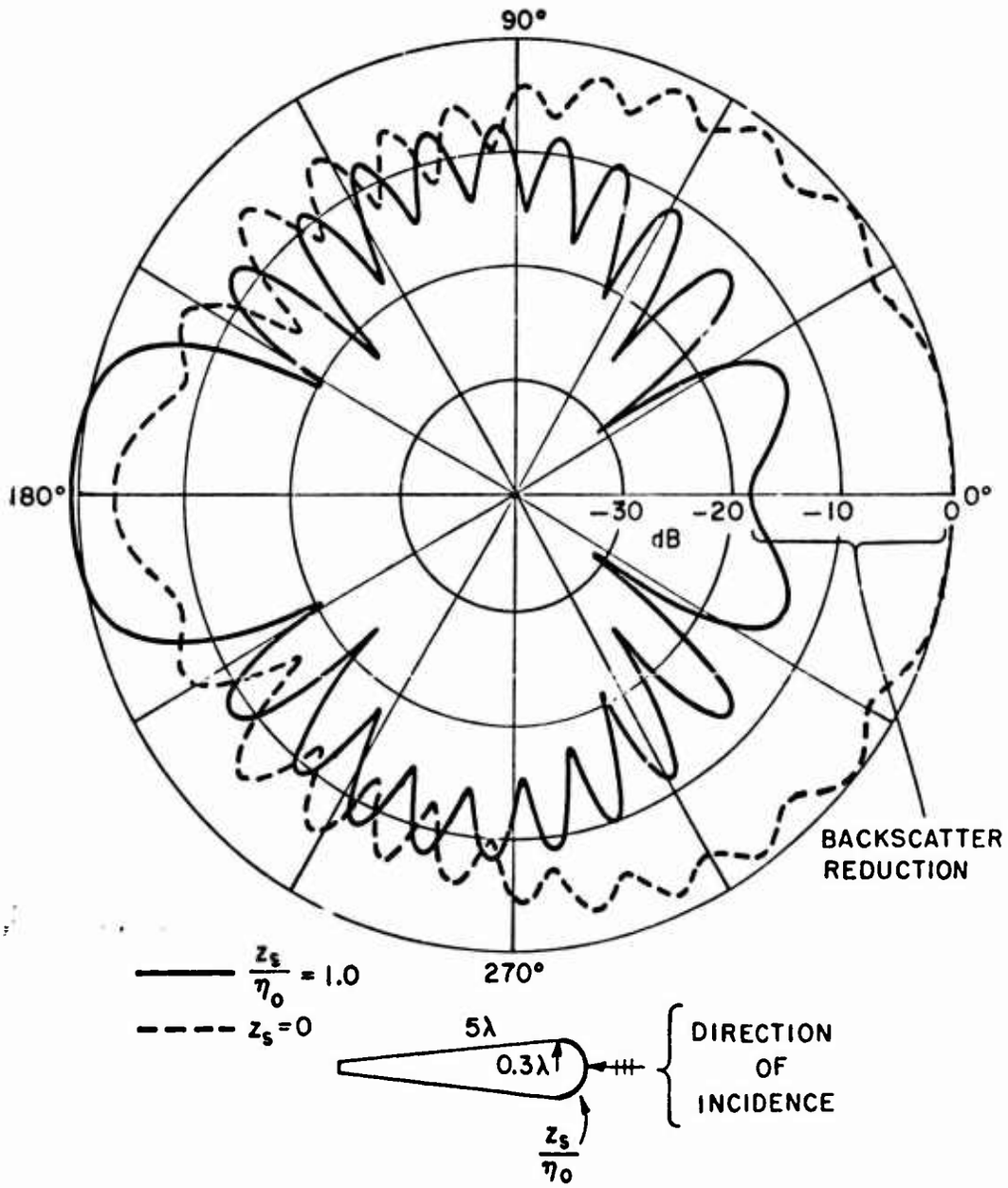

Fig. 26--Comparison of bistatic scattered fields for wings with and without impedance loading.

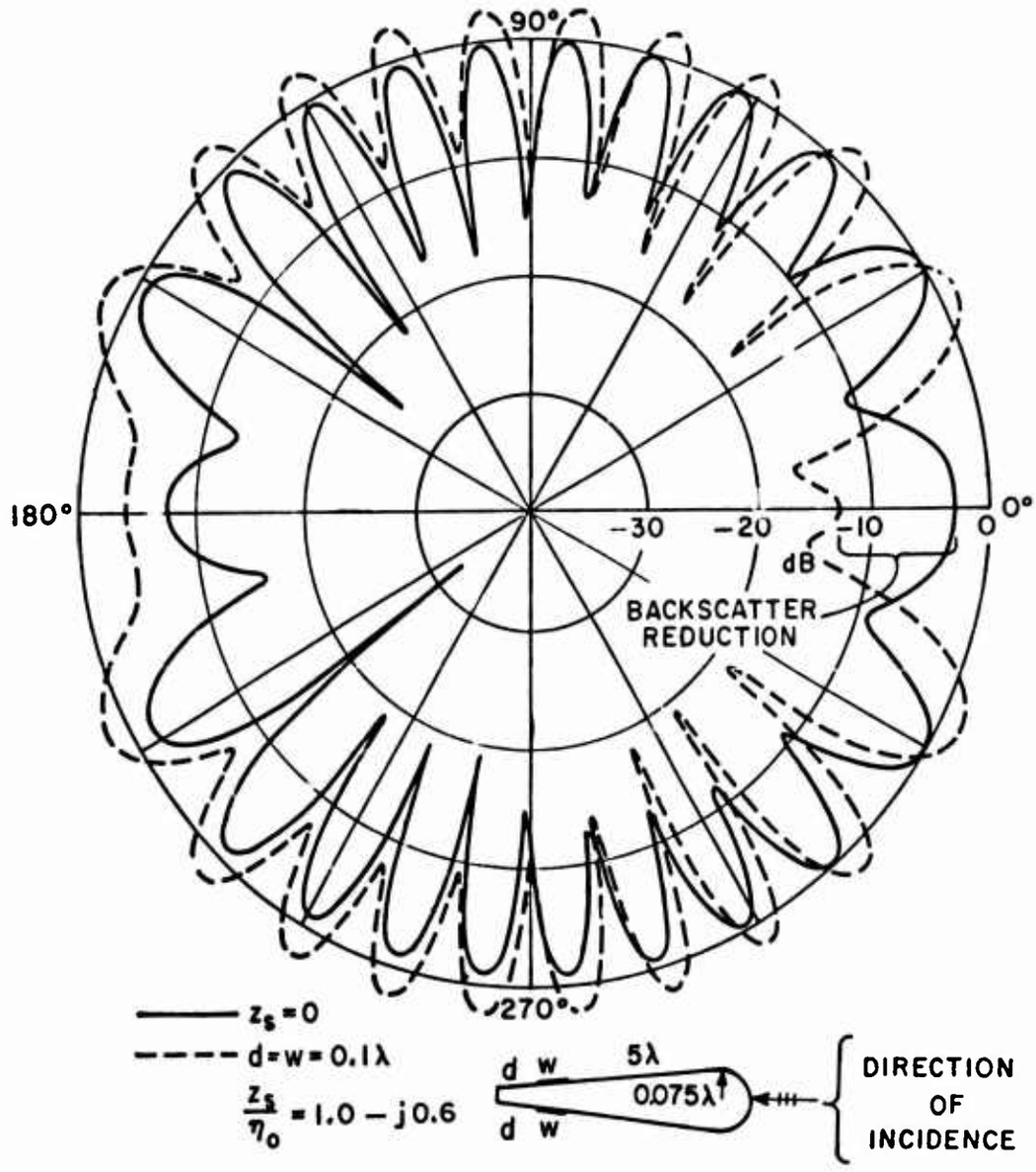

Fig. 27--Comparison of bistatic scattered fields for wings with and without impedance loading.

TABLE IV

BACKSCATTER REDUCTION OF WING MODEL AS A FUNCTION OF INCIDENCE ANGLE

Incidence Angle (θ)	Backscatter Reduction (dB)
0	18.00
3	17.57
8	16.47
10	12.08

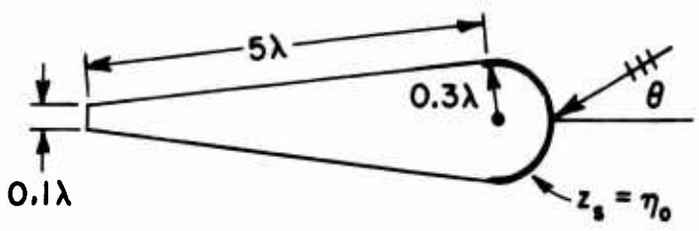

TABLE V

BACKSCATTER REDUCTION OF WING MODEL AS A FUNCTION ON INCIDENCE ANGLE

Incidence Angle (θ)	Backscatter Reduction (dB)
0	10.19
5	11.13
10	3.12

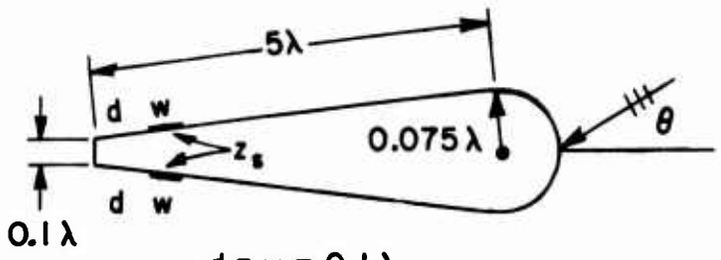

$$d = w = 0.1\lambda$$

$$\frac{z_s}{\eta_0} = 1.0 - j \cdot 0.6$$

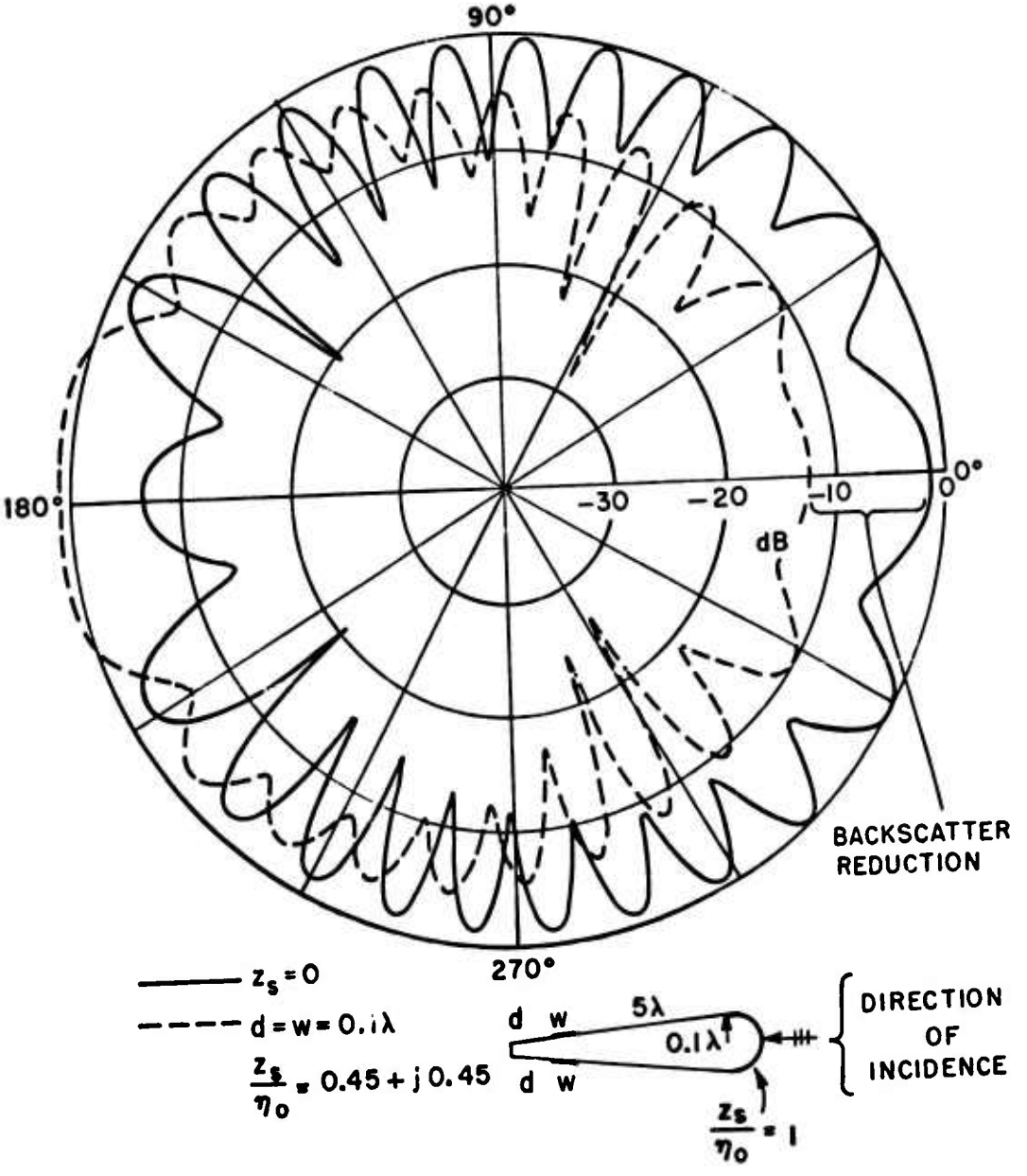

Fig. 28--Comparison of bistatic scattered fields for wings with and without impedance loading.

F. The Thin Strip

The infinitely long thin strips of 1 and 2 wavelength wide and 0.1 wavelength thick are studied by moment method. The backscatter reduction will be used to check the results obtained from a three-dimensional finite thin plate discussed in Chapter V. Typical results for 1 and 2 wavelength strips loaded with a 0.1λ wide surface impedance are shown in Figs. 29 and 30. Tables VI and VII show the backscatter reduction as a function of incidence angle.

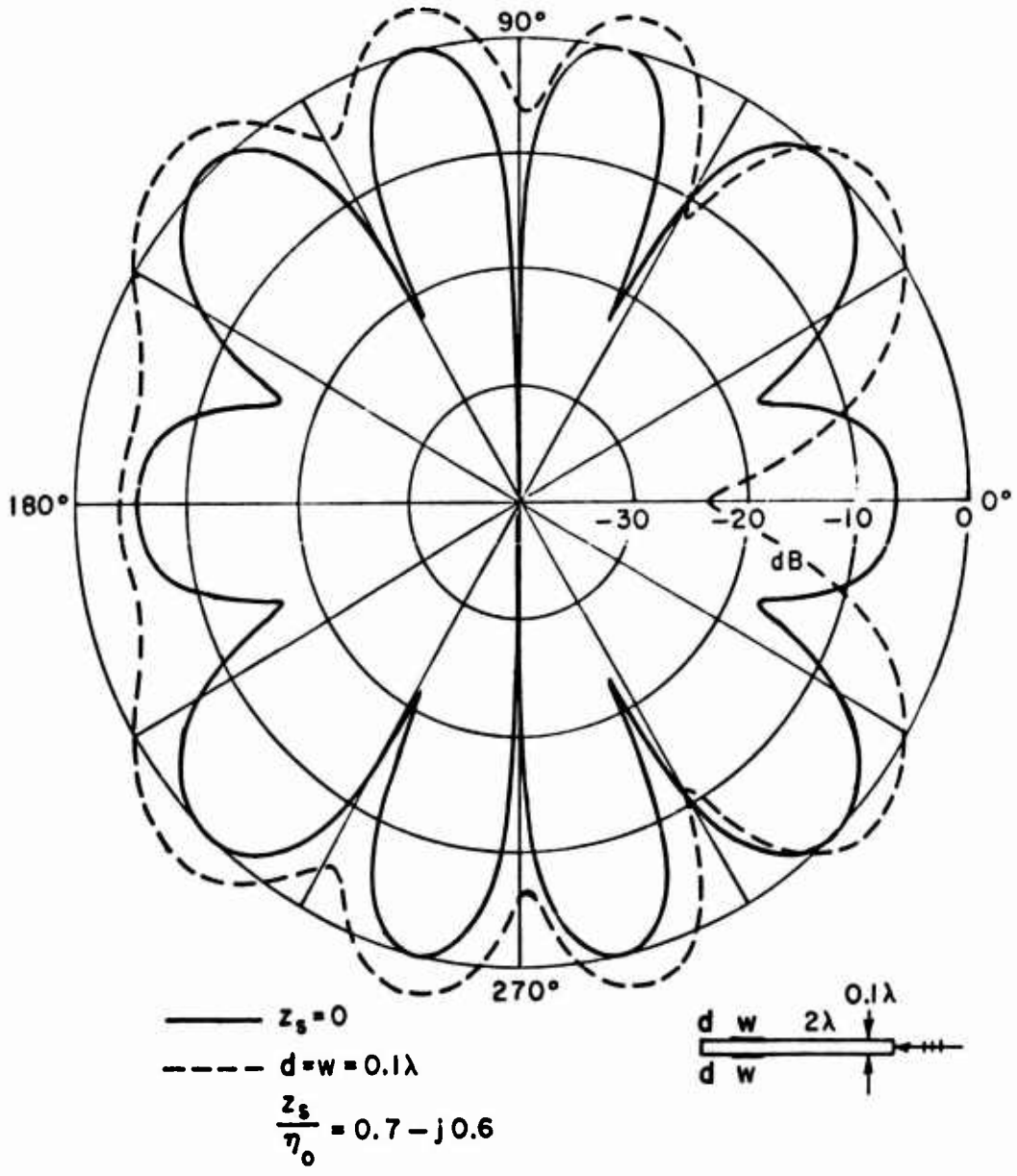

Fig. 29--Comparison of bistatic scattered fields for strips with and without impedance loading.

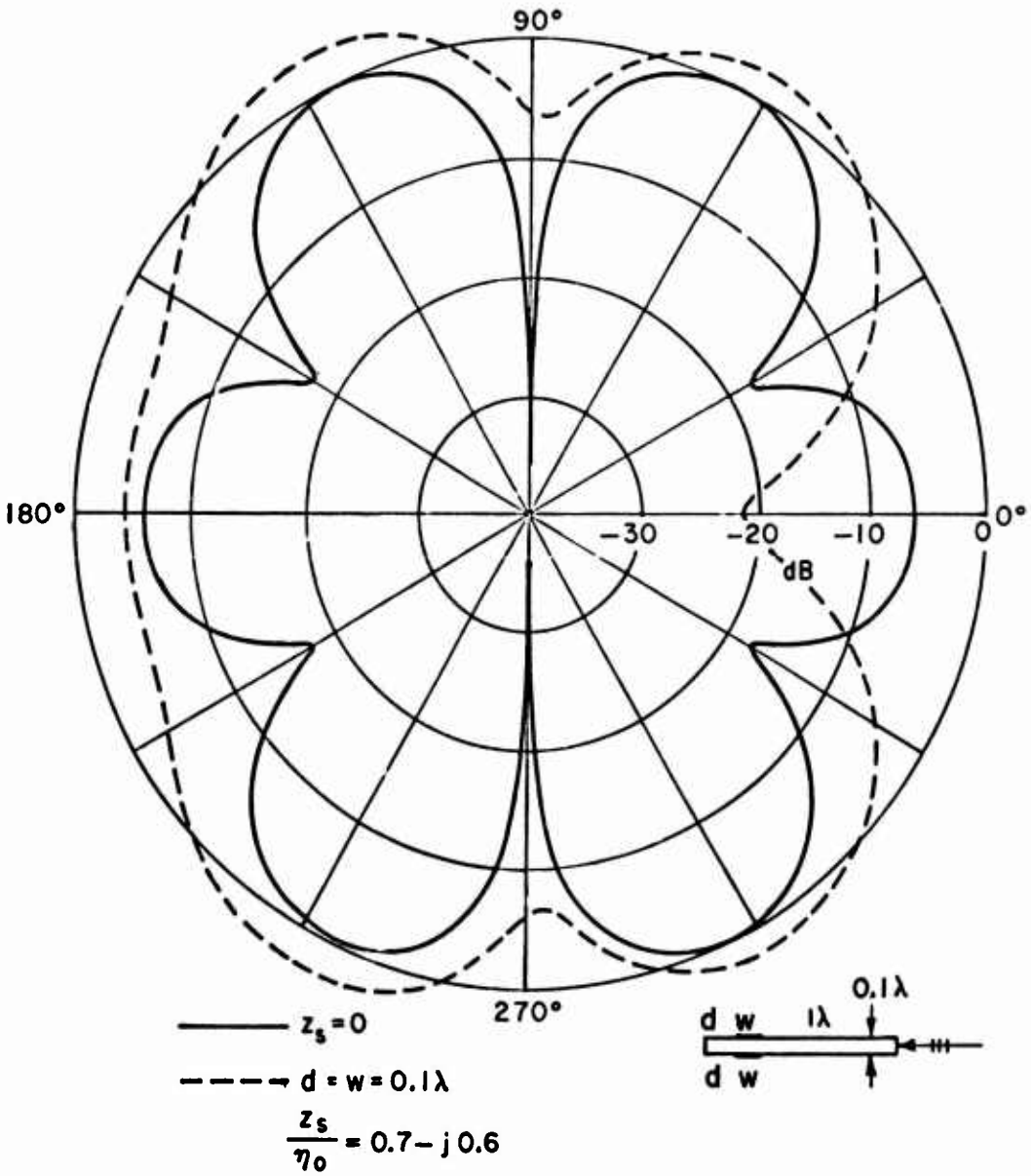

Fig. 30--Comparison of bistatic scattered fields for strips with and without impedance loading.

TABLE VI

BACKSCATTER REDUCTION OF THIN STRIP AS A FUNCTION OF INCIDENCE ANGLE

Incidence Angle (θ)	Backscatter Reduction (dB)
0	15.61
3	14.97
5	13.83
10	8.97

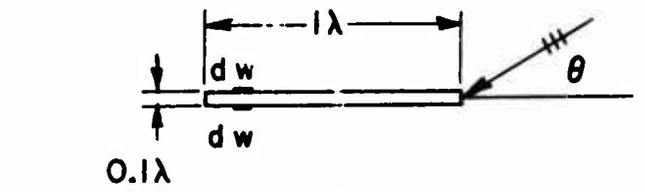

$d = w = 0.1\lambda$ $\qquad \frac{z_s}{\eta_o} = 0.7 - j \cdot 0.6$

TABLE VII

BACKSCATTER REDUCTION OF THIN STRIP AS A FUNCTION OF INCIDENCE ANGLE

Incidence Angle (θ)	Backscatter Reduction (dB)
0	16.45
3	15.89
5	13.39
10	5.45

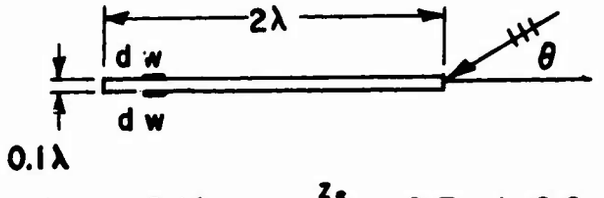

$d = w = 0.1\lambda$ $\qquad \frac{z_s}{\eta_o} \simeq 0.7 - j \cdot 0.6$

CHAPTER V

THE REDUCTION OF BACKSCATTERED FIELD --- THREE-DIMENSIONAL CASE

A. Introduction

The results previously discussed yield the necessary surface impedance loadings required to achieve reduction in the backscatter. However, a way to practically implement the required surface impedance is also needed. One of the most promising ways to implement the surface impedance is a collinear array of rectangular slots located along the edge.

In this chapter, the thin conducting plate with a loaded slot is treated. The reductions in backscatter of various sizes of plates are also illustrated. It is concluded that the backscatter reduction can be achieved over a 2:1 frequency band in a wide angular aspect.

B. The Thin Plate

Since the thin square plate with a loaded slot antenna can provide the information about the effect of loading, the backscatter reduction of the plate is investigated. For near grazing angles of incidence, the trailing edge of the plate is the dominant contributor to the scattering of the component of the electric field which is normal to the edge (vertical polarization). On the other hand, the leading edge contribution is the dominant factor to the scattering of the component of the electric field which is parallel to the edge (parallel polarization).

The reduction of the backscatter of the plate for the vertical polarization can be achieved by inserting a slot sufficiently near the trailing edge of the plate. The axis of the slot should be oriented parallel to the trailing edge in order for the slot to have maximum effect. A lumped load impedance may be inserted in the slot to tune the slot. The size, location and the load impedance of the slot have to be chosen properly in order to achieve a reduction in backscattering cross section over a wide frequency band.

The backscattering analysis for the plate with loaded slot has been carried out by approximating the conducting plate with a slot by a conducting wire grid model. The integral equations for the scattering of electromagnetic plane wave by the wire grid structure are then solved by the numerical techniques. A typical wire grid model of a half-wave slot in one wavelength square plate is illustrated in Fig. 31. The lumped load impedance of the slot antenna is obtained by

inserting a proper terminal load impedance at the center c of the wire segment abc in Fig. 31.

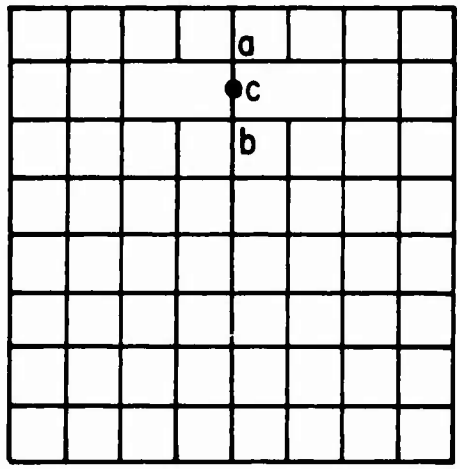

Fig. 31--Conducting wire grid model of a half-wavelength long slot in a one wavelength square conducting plate.

The wire-grid structure is considered as an array of thin wire segments. Current-sampling points or terminals are defined at each wire junction.

Assume that each segment in the wire structure has a circular cylindrical surface and the wire radius "a" is much smaller than the wavelength λ, and the wire length is much greater than the radius. Furthermore, the circumferential component J_ϕ of the surface current density will be neglected. If we consider the axial component of the surface current density to be independent of ϕ, then the surface current density of the thin wire structure is given by

$$(40) \qquad \vec{J}_s(\ell) = \frac{\hat{\ell} I(R)}{2\pi a} = \frac{\vec{I}(\ell)}{2\pi a}$$

where ℓ is the coordinate along the wire axis and $I(\ell)$ is the total current. Substituting Eq. (40) into Eq. (8) and using the impedance boundary condition of Eq. (9) leads to

$$(41) \qquad -\int_0^L I(\ell)\,(E_\ell^m - Z_s H_\phi^m)\,d\ell = V_m$$

where L denotes the overall wire length and

$$(42) \qquad V_m = \iiint (\vec{J}_i \cdot \vec{E}^m - \vec{M}_i \cdot \vec{H}^m)\,dv$$

$$(43) \qquad E_\ell^m = \frac{1}{2\pi} \int_0^{2\pi} \hat{\ell} \cdot \vec{E}^m \, d\phi$$

$$(44) \qquad H_\phi^m = \frac{1}{2\pi} \int_0^{2\pi} \hat{\phi} \cdot \vec{H}^m \, d\phi \quad .$$

In order to solve for the unknown current distribution in Eq. (41), a sinusoidal dipole is used as a test source. The current distribution on a V test dipole is

$$(45) \qquad \vec{F}(\ell) = \frac{\hat{\ell}_1 P_1 \sinh \gamma(\ell - \ell_1)}{\sinh \gamma \ell_1} + \hat{\ell}_2 \frac{P_2 \sinh \gamma(\ell_2 - \ell)}{\sinh \gamma \ell_2}$$

where P_1 and P_2 are unit pulse functions and

$$\gamma = j\omega\sqrt{\mu\varepsilon}$$

The current distribution on the wire structure is expanded in a finite series of sinusoidal functions,

$$(46) \qquad \vec{I}(\ell) = \sum_{n=1}^{N} I_n \vec{F}_n(\ell) \quad .$$

Substituting Eq. (46) into Eq. (41) gives

$$(47) \qquad \sum_{n=1}^{N} I_n Z_{mn} = V_m \qquad m = 1,2 \ldots N$$

where

$$(48) \qquad Z_{mn} = -\int_n F_n(\ell)\ (E_\ell^m - Z_s H_\phi^m)d\ell \quad .$$

Equation (47) can be solved for the unknown current I_n by numerical techniques.

If a lumped impedance Z_m is inserted at the m^{th} current sampling points of the wire structure, there is a voltage drop $I_m Z_m$ across the load. Therefore, in the delta gap model, the lumped loads simply introduce a new term in Eq. (47) so the right-hand side becomes $V_m - I_m Z_m$. Transferring the last term, we obtain

$$(49) \qquad \sum_{n=1}^{N} I_n(Z_{mn} + Z_m \delta_{mn}) = V_m \quad .$$

Once the current distribution is solved, the scattered field can be readily calculated.

The main computer program for the analysis of the backscattering of a plate is based on the computer subroutines developed by Richmond [33]. In order to model the plate with slot accurately, it is found that the spacing between wire grid should be as small as $\lambda/8$, at least in the vicinity of the slot.

The plate with a slot can be considered as an antenna. Using the compensation thecrem and the superposition principle, the scattered field from a loaded antenna may be interpreted as a load independent term called the structural scattering plus a load dependent term called the antenna mode scattering (see Appendix A).

The backscattering patterns in the plane perpendicular to the slot axis are calculated for different sizes of plates and slots using various load impedances. From Eq. (52) (see Appendix A) we see that if the short and open circuit scattered field from a loaded antenna are known (either measured or calculated) the scattered field for arbitrary load can be readily calculated. This is brought to the author's attention by Richmond [40]. Considerable amount of computer time can be saved by using Eq. (52) to find the optimum load impedance for backscatter reduction. The backscattered field calculated by directly using the wire-grid model is compared with that obtained by Eq. (52), as shown in Table VIII and IX. The reductions of back-scatter are shown in Figs. 32-37. The load impedance which is required

to reduce the backscatter from the trailing edge of the square plate over a 2:1 frequency band is plotted on a Smith chart in Fig. 38. It is seen from Figs. 32-37 that a substantial reduction (> 15 dB) in the backscattering cross section can be achieved when the slot is properly loaded. In order to achieve backscattering reduction for near grazing incidence on either edge, two slots, one on each edge, were used on the square plate. It is seen from Fig. 37 that the reduction obtained by using two slots is nearly as good as that for one slot.

TABLE VIII

COMPARISON OF THE SCATTERED FIELD OF A LOADED SQUARE PLATE

$0.5\lambda \times 0.5\lambda$ Plate, $Z_L = 14.87 - j.200$

	Calculated by Wire-Grid Model		Calculated by Eq. (52)	
θ	Real Part	Imaginary Part	Real Part	Imaginary Part
0	0.0	0.0	0.00000	0.00000
5	-0.00099	-0.00165	- .00098	- .00168
10	-0.00413	-0.00652	- .00412	- .00654
15	-0.00994	-0.01428	- .00992	- .01428
20	-0.01924	-0.02430	- .01925	- .02431
25	-0.03300	-0.03553	- .03303	- .03555
30	-0.05215	-0.04635	- .05212	- .04638
35	-0.07730	-0.05449	- .07731	- .05453
40	-0.10832	-0.05709	- .10833	- .05711
45	-0.14388	-0.05094	- .14390	- .05091
50	-0.18115	-0.03302	- .18110	- .03298
55	-0.21556	-0.00130	- .21549	- .00128
60	-0.24136	0.04435	- .24135	.04437
65	-0.25229	0.10127	- .25226	.10131
70	-0.24316	0.16376	- .24306	.16377
75	-0.21145	0.22357	- .21134	.22359
80	-0.15863	0.27131	- .15851	.27129
85	-0.09059	0.29873	- .09049	.29861
90	-0.01672	0.30089	- .01663	.30077
95	0.05215	0.27770	.05221	.27751
100	0.10646	0.23405	.10649	.23386
105	0.14020	0.17843	.14009	.17824
110	0.15206	0.12055	.15193	.12033
115	0.14515	0.06883	.14500	.06867
120	0.12536	0.02868	.12519	.02857
125	0.09940	0.00193	.09920	.00192
130	0.07303	-0.01260	.07283	- .01260
135	0.05005	-0.01787	.04988	- .01781
140	0.03220	-0.01732	.03208	- .01725
145	0.01958	-0.01395	.01954	- .01387
150	0.01133	-0.00987	.01128	- .00977
155	0.00627	-0.00626	.00620	- .00623
160	0.00329	-0.00354	.00328	- .00352
165	0.00159	-0.00175	.00160	- .00171
170	0.00064	-0.00069	.00062	- .00067
175	0.00015	-0.00016	.00012	- .00019

TABLE IX

COMPARISON OF THE SCATTERED FIELD OF A LOADED SQUARE PLATE

$0.6\lambda \times 0.6\lambda$ Plate, $Z_L = 56.16 - j.300$

	Calculated by Wire-Grid Model		Calculated by Eq. (52)	
θ	Real Part	Imaginary Part	Real Part	Imaginary Part
0	0.0	0.0	0.00000	0.00000
5	-0.00117	-0.00207	- .00117	- .00206
10	-0.00489	-0.00815	- .00488	- .00817
15	-0.01180	-0.01790	- .01179	- .01788
20	-0.02291	-0.03059	- .02292	- .03058
25	-0.03948	-0.04503	- .03948	- .04502
30	-0.06282	-0.05934	- .06282	- .05936
35	-0.09400	-0.07082	- .09400	- .07082
40	-0.13337	-0.07582	- .13336	- .07583
45	-0.17991	-0.06990	- .17992	- .06990
50	-0.23051	-0.04823	- .23052	- .04822
55	-0.27933	-0.00665	- .27934	- .00663
60	-0.31763	0.05672	- .31762	.05675
65	-0.33470	0.13953	- .33465	.13950
70	-0.32014	0.23350	- .32011	.23345
75	-0.26748	0.32433	- .26747	.32423
80	-0.17801	0.39394	- .17806	.39378
85	-0.06290	0.42539	- .06305	.42521
90	0.05809	0.40886	.05783	.40870
95	0.16177	0.34612	.16140	.34607
100	0.22891	0.25106	.22845	.25113
105	0.25057	0.14527	.25013	.14555
110	0.23041	0.05077	.23007	.05121
115	0.18207	-0.01702	.18190	- .01646
120	0.12317	-0.05287	.12320	- .05228
125	0.06903	-0.06094	.06920	- .06040
130	0.02873	-0.05091	.02902	- .05048
135	0.00458	-0.03327	.00492	- .03297
140	-0.00609	-0.01603	- .00575	- .01586
145	-0.00809	-0.00345	- .00780	- .00337
150	-0.00601	0.00351	- .00578	.00351
155	-0.00310	0.00587	- .00293	.00583
160	-0.00094	0.00536	- .00083	.00531
165	0.00008	0.00362	.00013	.00360
170	0.00026	0.00177	.00029	.00176
175	0.00010	0.00046	.00009	.00045

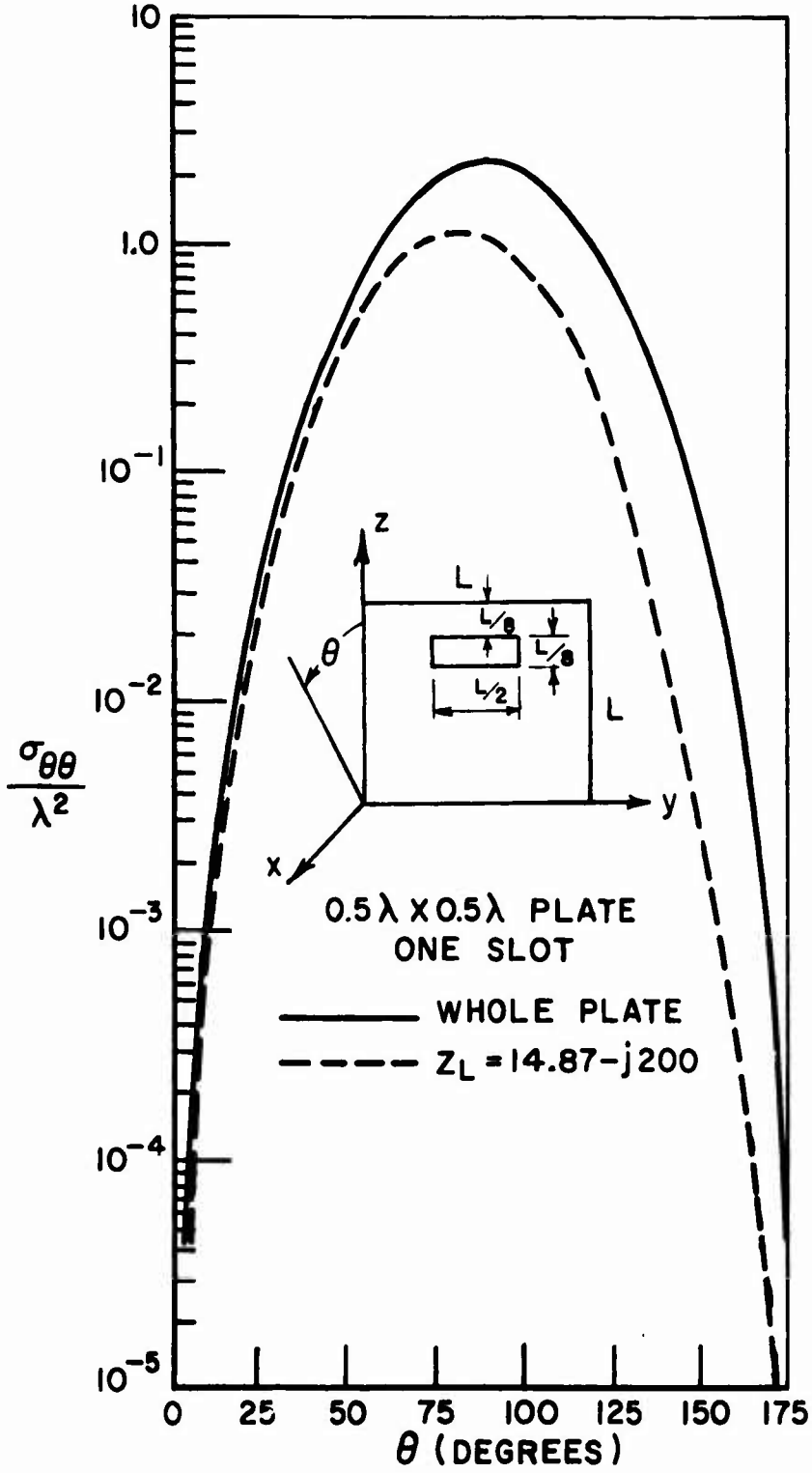

Fig. 32--Use of a loaded slot for reduction of an edge diffracted field from a flat plate.

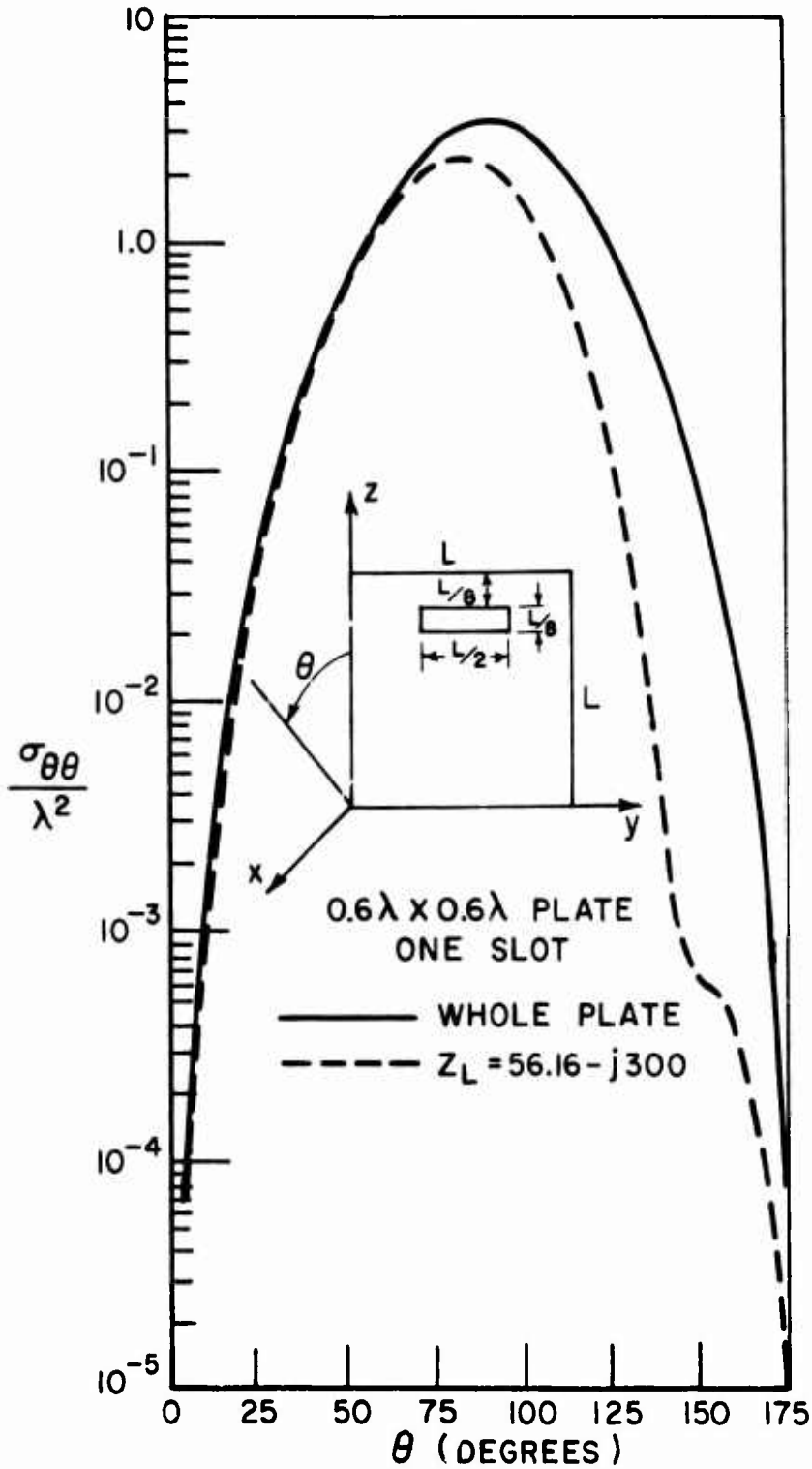

Fig. 33--Use of a loaded slot for reduction of an edge diffracted field from a flat plate.

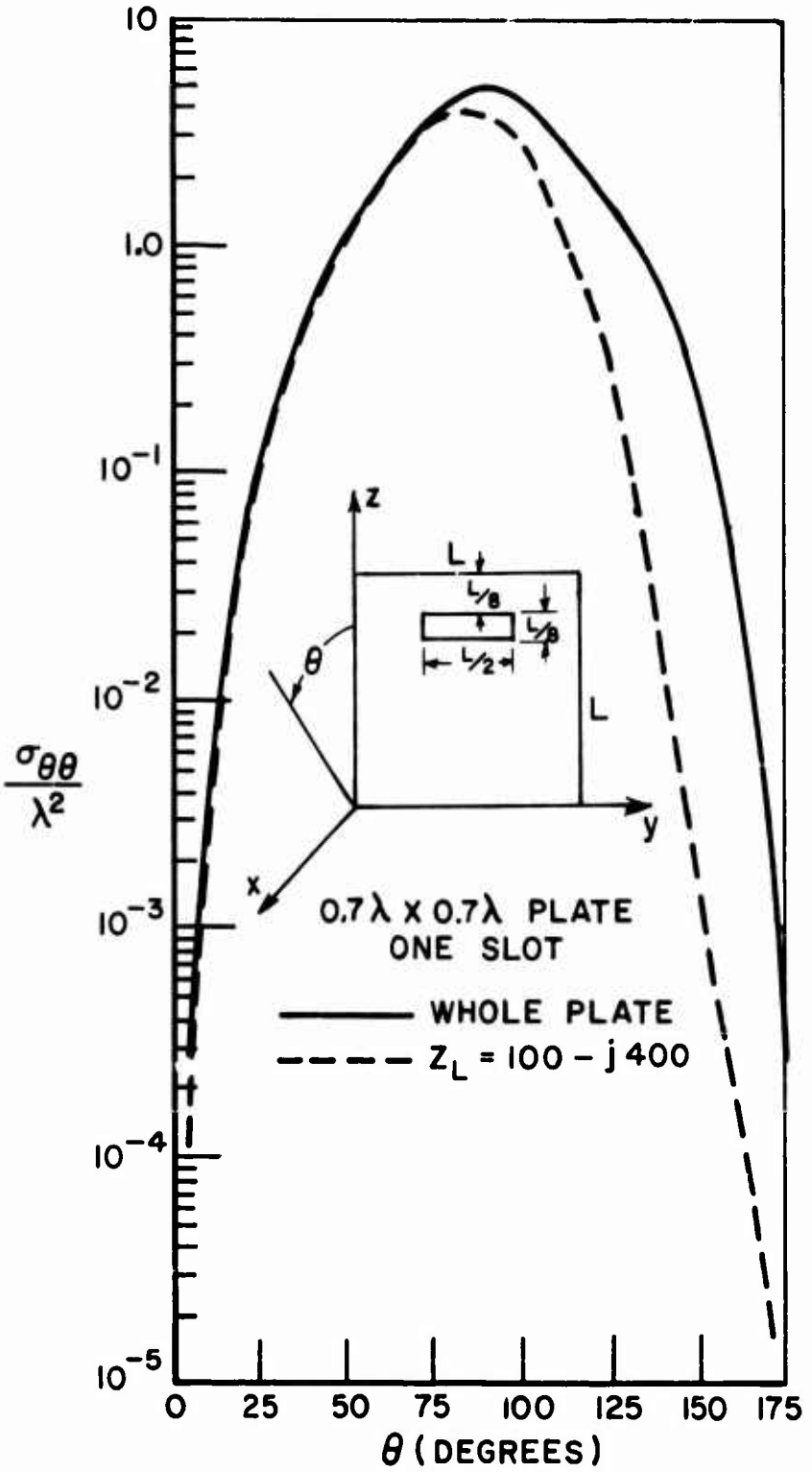

Fig. 34--Use of a loaded slot for reduction of an edge diffracted field from a flat plate.

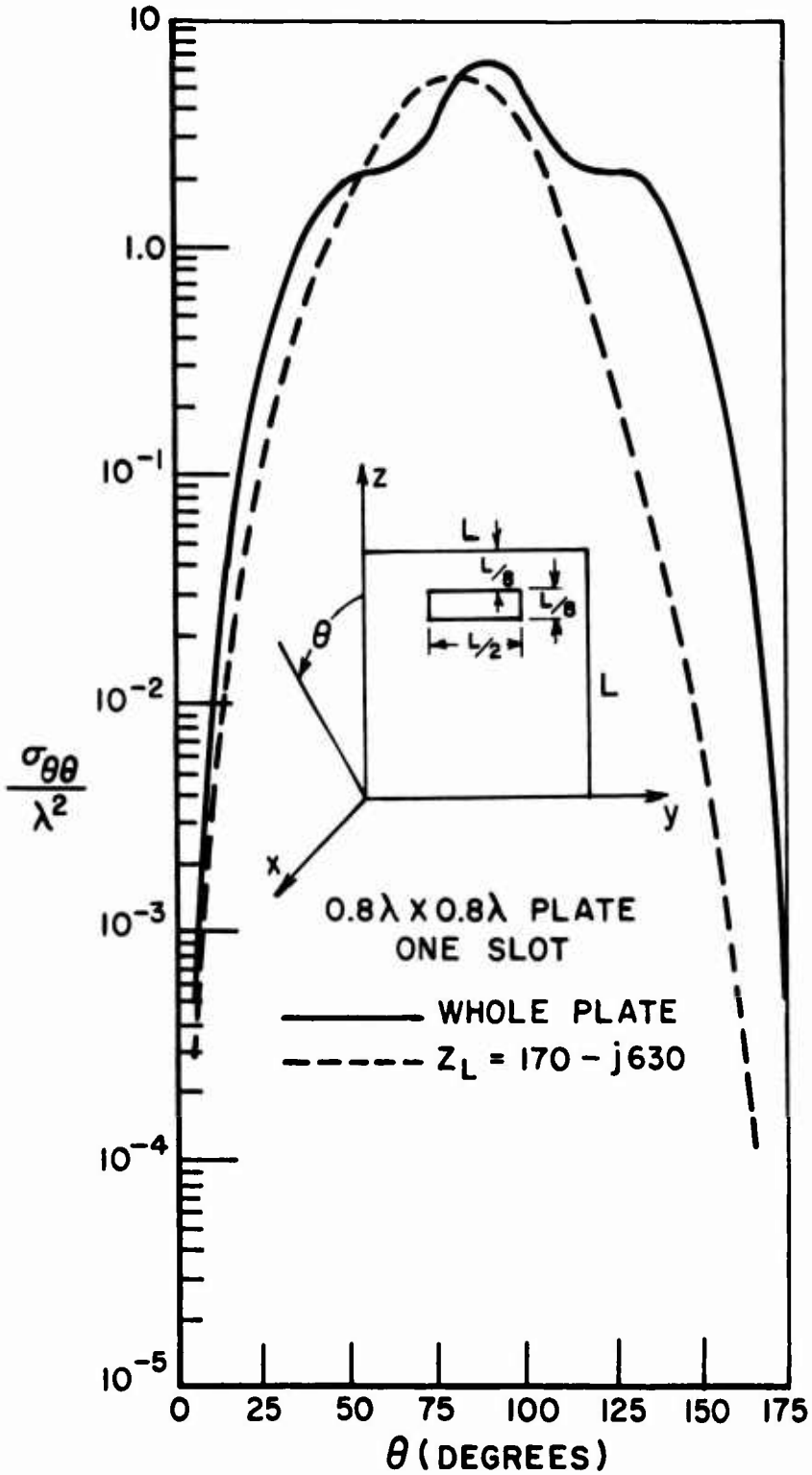

Fig. 35--Use of a loaded slot for reduction of an edge diffracted field from a flat plate.

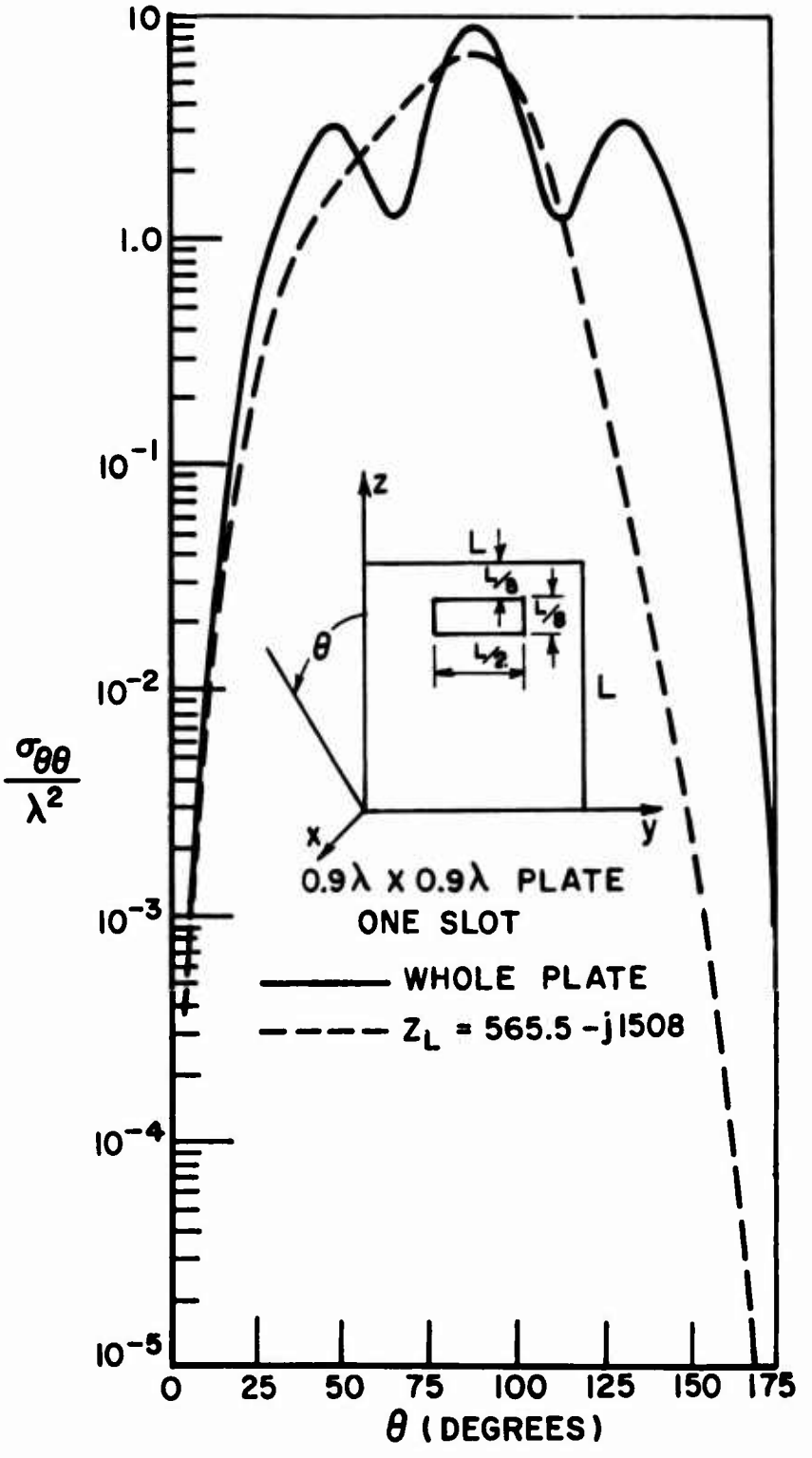

Fig. 36--Use of a loaded slot for reduction of an edge diffracted field from a flat plate.

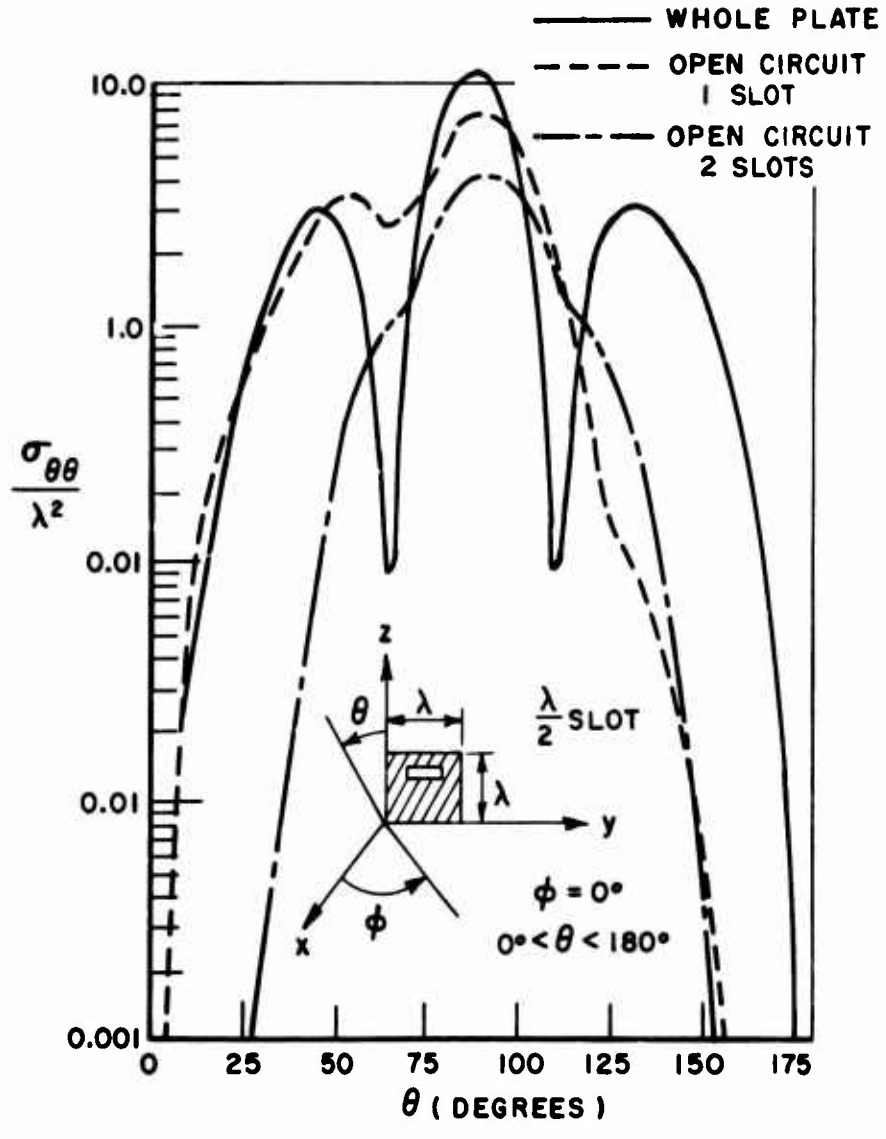

Fig. 37. Backscattering cross section ($\sigma_{\theta\theta}/\lambda^2$ for the $\hat{\theta}$ polarization) of a square conduction plate with one and two slots.

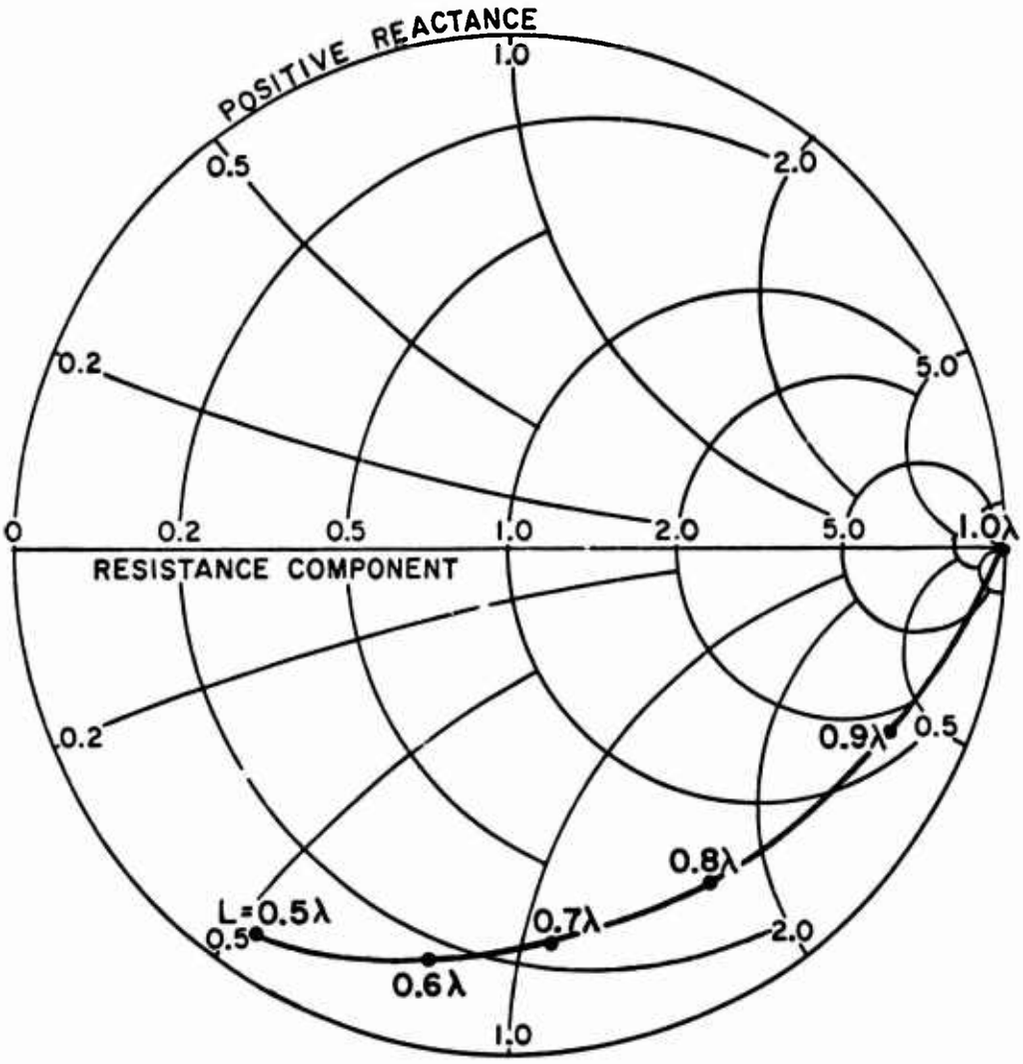

Fig. 38--Load impedance required for reduction of wedge diffracted backscattered fields.

CHAPTER VI

CONCLUSIONS

The application of impedance loading techniques for the reduction of backscatter from radar targets were studied. The hybrid methods which combine the GTD and the moment method were used to analyze the backscattering from various geometries such as the impedance-loaded infinite wedge, thin strip and a two-dimensional wing model. The surface impedance was used to simulate a slot antenna loaded with a terminal impedance. The original hybrid method was found inadequate to analyze the reduction in scattering by edge loading an infinite wedge. A solution to this difficulty was attained by the development of the ΔJ method.

The effect of the edge diffraction sources can be considerably reduced over a 3:1 frequency band by the use of a loaded slot near or at an edge. These reductions are found to cover an angular range of 20° from grazing.

In order to include the effect of the leading edge, a two-dimensional wing model which provides a good simulation of a practical aircraft wing cross section was also studied. The backscatter reductions for the wing model were calculated as a function of wing size and geometry.

The slot-loaded square plate which is a basis of an array of finite slots along the edge of a three-dimensional wing model was analyzed by a wire grid model. The array of loaded slots is one of the most promising ways to implement the necessary surface impedance loadings required to achieve reductions in the backscatter. The backscatter reduction of the square plate can be achieved at least over a 2:1 frequency band. It is also demonstrated that the use of two slots on the plate can reduce the backscattering for near grazing incidence on either edge.

APPENDIX A

THE SCATTERED FIELD OF AN ANTENNA AS A FUNCTION OF LOAD IMPEDANCE

The scattered field from an impedance-loaded object can be expressed as a superposition of the field scattered by the unloaded object and the field reradiated by the load. In attempting to predict the scattered field from an antenna as a function of the load impedance many researchers have presented different functional forms [8,35,36,37,38,39]. In the form discussed here, the scattered field can be interpreted as a load independent term called the structural scattering plus a term called antenna mode scattering.

Consider the scattering of electromagnetic wave by an impedance-loaded antenna as shown in Fig. 39. Using the compensation theorem, the load may be replaced by a voltage source. By superposition principle, the scattered field is broken into two parts, one due to the incident field on the shorted antenna and the other to the equivalent voltage source exciting the antenna. Therefore, the scattered field by an antenna as a function of the load impedance is given by

$$\vec{E}(Z_\ell) = \vec{E}(0) - \frac{Z_\ell}{Z_\ell + Z_a} I(0)\vec{E}^r \tag{50}$$

where

$\vec{E}(0)$ = the field scattered by the antenna with $Z_\ell = 0$, that is, a short circuit for the load,

$I(0)$ = the antenna terminal current with $Z_\ell = 0$,

$\vec{E}^r$ = the field radiated by the antenna when excited by a unit current source,

and

Z_a, Z_ℓ are antenna and load impedance, respectively.

Let the load impedance approach infinity, that is, open circuit, then Eq. (50) becomes

$$\vec{E}(\infty) = \vec{E}(0) - I(0)\vec{E}^r$$

or

$$I(0)\vec{E}^r = \vec{E}(0) - \vec{E}(\infty) \; . \tag{51}$$

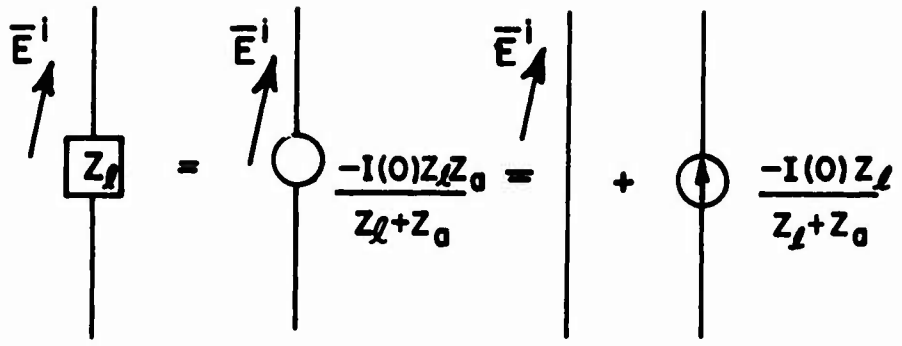

Fig. 39--Compensation and superposition theorem applied to scattering problem.

Substituting Eq. (51) into Eq. (50) gives

$$\vec{E}(Z_\ell) = \vec{E}(0) - \frac{Z_\ell [\vec{E}(0) - \vec{E}(\infty)]}{Z_\ell + Z_a} \tag{52}$$

$$= \frac{Z_a \vec{E}(0) + Z_\ell \vec{E}(\infty)}{Z_\ell + Z_a}$$

Equation (52) can be used to calculate the scattered field for arbitrary load if the open and short circuit scattered field from the antenna are known.

REFERENCES

[1] E. Meyer and H. Severin, "Absorption Sanordnugen by Electromagnetische Zentimeterwetten und ihre Akastische Analogien," Z. Angew. Phys., Vol. 8, pp. 105-114, March 1956.

[2] V. Muller, "Absorption and Transmission of Electromagnetic Waves, Phase G: Absorbent Coating on Metal Cylinders," Rome Air Development Center Tech. Rept. TDR-62-21, 1960. (AD 271-796)

[3] V. H. Weston, "Theory of Absorbers in Scattering," IEEE Trans. on Antenna and Propagation, Vol. AP-11, pp. 578-584, September 1963.

[4] V. H. Weston and J. J. Bowman, "Some Remarks Concerning the Design of Absorbers in Resonance Region," IEEE Trans. on Antenna and Propagation, Vol. AP-13, pp. 467-468, May 1965.

[5] E. F. Knott, V. V. Liepa and T. B. A. Senior, "Nonspecular Radar Cross Section Study," The University of Mighigan Radiation Laboratory Report No. 011062-1-F (AFAL-TR-73-70), April 1973.

[6] E. F. Knott and T. B. A. Senior, "Non-specular Radar Cross Section Study," The University of Michigan Radiation Laboratory Report No. 011062-1-T (AFAL-TR-73-2), February 1973.

[7] E. F. Knott and T. B. A. Senior, "Non-specular Radar Cross Section Study," The University of Michigan Radiation Laboratory Report No. 011764-1-T (AFAL-TR-73-422), January 1974.

[8] J. K. Schindler, R. B. Mack and P. Blacksmith, Jr., "The Control of Electromagnetic Scattering by Impedance Loading," Proc. of the IEEE, Vol. 53, pp. 993-1004, August 1965.

[9] L. Weinberg, "New Techniques for Modifying Monostatic and Multistatic Radar Cross Section," IEEE Trans. on Antenna and Propagation, Vol. AP-11, pp. 717-719, November 1963.

[10] K. M. Chen and V. Leipa, "The Minimization of the Back Scattering of a Cylinder by Central Loading," IEEE Trans. on Antenna and Propagation, Vol. AP-12, pp. 572-582, September 1964.

[11] M. A. Leontovich, "Investigation of Propagation of Radio Waves, Part II," Moscow 1948.

[12] T. B. A. Senior, "Impedance Boundary Conditions for Imperfectly Conducting Surfaces," Appl. Sci. Res., Section B, Vol. 8, 1960, pp. 418-436.

[13] T. B. A. Senior, " A Note on Impedance Boundary Conditions," Can. J. Phys., Vol. 40, 1962, pp. 663-665.

[14] V. H. Rumsey, "Reaction Concept in Electromagnetic Theory," Physical Review, Vol. 94, June 15, 1954, pp. 1483-1491.

[15] M. H. Cohen, "Application of the Reaction Concept to Scattering Problems," IEEE Trans., Vol. AP-3, October 1955, pp. 193-199.

[16] R. F. Harrington, Time-Harmonic Electromagnetic Fields, McGraw-Hill, New York, 1961, pp. 340-345.

[17] J. H. Richmond, "A Reaction Theorem and its Application to Antenna Impedance Calculations," IEEE Trans., Vol. AP-9, November 1961, pp. 515-520.

[18] S. A. Schelkunoff, "On Diffraction and Radiation of Electromagnetic Waves," Physical Review, Vol. 56, August 15, 1939.

[19] J. H. Richmond, "Radiation and Scattering by Thin-Wire Structures in the Complex Frequency Domain," Report 2902-10, July 1973, The Ohio State University ElectroScience Laboratory, Department of Electrical Engineering; prepared under Grant No. NGL 36-008-138 for National Aeronautics and Space Administration, Langley Research Center, Hampton, Va.

[20] R. F. Harrington, Field-Computation by Moment Methods, The Mac Millan Co., New York, 1968.

[21] A. Sommerfeld, Optics, Academic Press, Inc., New York, 1954, pp. 245-265.

[22] R. C. Rudduck, "Application of Wedge Diffraction to Antenna Theory," Report 1691-13, 30 June 1965, The Ohio State University ElectroScience Laboratory, Department of Electrical Engineering; prepared under Grant no. NSG-448 for National Aeronautics and Space Adminstration, Washington, D.C. (NASA Rpt. CR-372)

[23] W. Pauli, "An Asymptotic Series for Functions in the Theory of Diffraction of Light," Phys. Rev., Vol. 54, December 1938, pp. 924-931.

[24] D. L. Hutchins and R. G. Kouyoumjian, "A New Asymptotic Solution to the Diffraction by a Wedge," URSI 1967 Spring Meeting, Ottawa, pp. 154-155.

[25] D. L. Hutchins, "Asymptotic Series Describing the Diffraction of a Plane Wave by a Two-Dimensional Wedge of Arbitrary Angle," Ph.D. Dissertation, The Ohio State University, Department of Electrical Engineering, 1967.

[26] P. H. Pathak and R. G. Kouyoumjian, "The Dyadic Diffraction Coefficient for a Perfectly Conducting Wedge," Report 2183-4, 5 June 1970, The Ohio State University ElectroScience Laboratory, Department of Electrical Engineering; prepared under Contract AF 19(628)-5929 for Air Force Cambridge Research Laboratories. (AFCRL-69-0546) (AD 707 827)

[27] W. D. Burnside, C. L. Yu and R. J. Marhefka, "A Technique to Combine the Geometrical Theory of Diffraction and the Moment Method," 1973 GAP International Symposium, Boulder, Colorado, August 1973.

[28] W. D. Burnside, C. L. Yu and R. J. Marhefka, "A Technique to Combine the Geometrical Theory of Diffraction and the Moment Method," Short Course Notes, The Ohio State University ElectroScience Laboratory, Department of Electrical Engineering, September 10-14, 1973.

[29] M. G. Andreasen, "Scattering from Cylinders with Arbitrary Surface Impedance," Proc. of IEEE, Vol. 53, 1965, pp. 812-817.

[30] J. H. Richmond, "An Integral-Equation Solution for TE Radiation and Scattering from Conducting Cylinders," Report 2902-7, October 1972, The Ohio State University ElectroScience Laboratory; Department of Electrical Engineering; prepared under Grant No. NGL 36-008-138 for National Aeronautics and Space Administration, Langley Research Center, Hampton, Va.

[31] R. F. Harrington and J. R. Mautz, "Control of Radar Scattering by Reactive Loading," IEEE Trans. on Antenna and Propagation, Vol. AP-20, pp. 446-454, July 1972.

[32] R. B. Green, "The Echo Area of Small Rectangular Plates with Linear Slots," IEEE Trans. on Antenna and Propagation, Vol. AP-12, pp. 101-104, January 1964.

[33] J. H. Richmond, "Computer Programs for Thin-Wire Structures in a Homogeneous Conducting Medium," Report 2902-12, August 1973, The Ohio State University ElectroScience Laboratory, Department of Electrical Engineering; prepared under Grant No. NGL 36-008-138 for National Aeronautics and Space Administration, Langley Research Center, Hampton, Va.

[34] J. B. Keller, "Geometrical Theory of Diffraction," Journal of the Optical Society of America, Vol. 52, pp. 116-130, February 1962.

[35] R.W.P. King, and C.W. Harrison, Jr., "The Receiving Antenna," Proc. I.R.E., No. 32, January 1944, p. 35.

[36] A. F. Stevenson, "Relations Between the Transmitting and Receiving Properties of Antennas," Quarterly of Applied Mathematics, Vol. 5, January 1948, pp. 140-148.

[37] R. J. Garbacz, "Determination of Antenna Parameters by Scattering Cross-section Measurements," Proc. IEE (London), Vol. 111, October 1964, pp. 1679-1686.

[38] E. M. Kennaugh, "The Echoing Area of Antennas," Report 601-14, December 1957, The Ohio State University ElectroScience Laboratory, Department of Electrical Engineering; prepared under Contract AF 33(616)-2546 for Wright Air Development Center, Wright-Patterson Air Force Base, Ohio. (AD 152 786)

[39] R. B. Green, "The General Theory of Antenna Scattering," Report 1223-17, November 1963, The Ohio State University ElectroScience Laboratory, Department of Electrical Engineering; prepared under Contract AF 33(616)-8039 for Wright-Patterson Air Force Base, Ohio. (AD 429 186)

[40] J. H. Richmond, private communication.

[41] P. M. Russo, R. C. Rudduck and L. Peters, Jr., "A Method for Computing E-plane Patterns of Horn Antennas," IEEE Trans. on Antennas and Propagation, AP-13, No. 2, March 1965, pp. 219-224.